Primate naïve pluripotent stem cells stall in the G1 phase of the cell cycle and differentiate prematurely during embryo colonization

Irène Aksoy[1,*], Cloé Rognard[1], Anaïs Moulin[1], Guillaume Marcy[1], Etienne Masfaraud[1], Florence Wianny[1], Véronique Cortay[1], Angèle Bellemin-Ménard[1], Nathalie Doerflinger[1], Manon Dirheimer[1], Chloé Mayère[1], Cian Lynch[4], Olivier Raineteau[1], Thierry Joly[2,3], Colette Dehay[1], Manuel Serrano[4], Marielle Afanassieff[1], and Pierre Savatier[1,*]

[1]Univ Lyon, Université Lyon 1, INSERM, Stem Cell and Brain Research Institute U1208, F-69500 Bron, France

[2]ISARA-Lyon, F-69007 Lyon, France

[3]VetAgroSup, UPSP ICE, F-69280 Marcy l'Etoile, France

[4]Cellular Plasticity and Disease Group, Institute for Research in Biomedicine (IRB Barcelona), Barcelona Institute of Science and Technology (BIST), Barcelona 08028, Spain

***Corresponding authors:**

Irène Aksoy (irene.aksoy@inserm.fr) and Pierre Savatier (pierre.savatier@inserm.fr)

Stem Cell and Brain Institute, INSERM U1208

18 Avenue du Doyen Lépine

F-69675 Bron Cedex

France

Material requests should be addressed to Irène Aksoy (irene.aksoy@inserm.fr).

Abstract

After reprogramming to naïve pluripotency, human pluripotent stem cells (PSCs) still exhibit very low ability to make interspecies chimeras in mice and pigs. Whether this is because they are inherently devoid of the attributes of chimeric competency or because naïve PSCs in general cannot colonize embryos from distant species remains to be elucidated. Here, we have used different types of mouse, human and rhesus monkey naïve PSCs and we have analyzed their ability to colonize both distant (rabbit) and close (cynomolgus monkey) embryos. Mouse embryonic stem cells (ESCs) remained mitotically active after injection into rabbit and cynomolgus embryos and contributed to the formation of the neural tube in post-implantation rabbit embryos. In contrast, primate naive PSCs colonized rabbit and cynomolgus embryos with much lower efficiency, regardless of the reprogramming protocols. Unlike mouse ESCs, they slowed DNA replication following colony dissociation and, after injection into host embryos, they stalled in the G1 phase of the cell cycle and differentiated prematurely, regardless of host species, distant or close. These results show that, unlike mouse ESCs, primate naive PSCs do not make chimeras because they are inherently unfit to stay mitotically active during embryo colonization.

Introduction

Human embryo-derived pluripotent stem cells (PSCs) and human induced PSCs (iPSCs) exhibit biological and functional characteristics of primed pluripotency: 1) dependence on fibroblast growth factor 2 (FGF2)/extracellular signal-regulated kinase and activin A/SMAD signaling for self-renewal; 2) inactivation of the 2nd X chromosome in female lines; and 3) a global transcriptome more similar to that of post-implantation epiblast in the gastrulation embryo (Nichols and Smith, 2009, Chen and Lai, 2014, Davidson et al., 2015, Nakamura et al., 2016). Although PSC lines obtained from rhesus monkeys are less well characterized, they also exhibit the essential characteristics of primed pluripotency (Wianny et al., 2008). In this respect, human and non-human primate PSCs differ from their murine counterparts, which exhibit biological and functional characteristics of naïve pluripotency (Nichols and Smith, 2009, Chen and Lai, 2014, Davidson et al., 2015). Notably, naïve and primed PSCs differ in their capacity to generate chimeras following injection into pre-implantation embryos. Although mouse ESCs (mESCs) produce germline chimeras, rhesus monkey PSCs do not colonize the ICM/epiblast of the host embryo and undergo apoptosis (Tachibana et al., 2012).

Different culture media with capacity to produce primed-to-naïve conversion of human, cynomolgus, and rhesus macaque PSCs have been reported. They use different combinations of transcription factors (Oct4, Krüppel-like factor [KLF]2, KLF4, NANOG, and STAT3), growth factors (LIF, activin A, transforming growth factor β [TGFβ], and FGF2), receptor agonist (lysophosphatidic acid) and antagonist (dorsomorphin), and chemical inhibitors of kinases (Rho kinase [ROCK], BRAF, p38/MAPK], glycogen synthase kinase 3 [GSK3], MEK1/2, SRC, protein kinase A, protein kinase C, RAF, and c-Jun N-terminal kinase) and of histone deacetylases (HDAC1 and HDAC2) [reviewed in (Collier and Rugg-Gunn, 2018, Li and Izpisua Belmonte, 2018)]. The media are variously termed naïve human stem cell media (NHSM) (Gafni et al., 2013), E-NHSM (https://hannalabweb. weizmann.ac.il), NHSM-v (Chen et al., 2015b), 3iL (Chan et al., 2013), Reset (Takashima et al., 2014), 5i/L/A, and 6i/L/A (Theunissen et al., 2014, Theunissen et al., 2016), 4i/L/b (Fang et al., 2014), TL2i (Chen et al., 2015a), 2iLD, 4i and FAC (Wu et al., 2017), t2iLGöY (Guo et al., 2017), and LCDM (Yang et al., 2017b). PSCs under these culture conditions display characteristic features of naïve state pluripotency of mESCs with a reconfigured transcriptome and epigenome (Huang et al., 2014, Chen et al., 2015a, Nakamura et al., 2016), loss of FGF2 dependency (Chen et al., 2015a,

Takashima et al., 2014), gain of STAT3 dependency (Gafni et al., 2013, Chan et al., 2013, Chen et al., 2015a, Takashima et al., 2014), reactivation of the second X-chromosome (Theunissen et al., 2014, Takashima et al., 2014, Fang et al., 2014), and elevation of oxidative phosphorylation (Ware et al., 2009, Takashima et al., 2014).

Colonization of mouse embryos by human naïve PSCs and their subsequent participation in germ layer differentiation has been reported (Gafni et al., 2013, Fang et al., 2014). However, these early results were not confirmed by subsequent reports: low rates of chimerism (<0.001%) in <1% of the fetuses were reported after injection of human naïve PSCs in mouse blastocysts (Masaki et al., 2015, Theunissen et al., 2016). Similarly, very low rates of chimerism were also observed in pig fetuses after injecting human naïve iPSCs in pig embryos (Wu et al., 2017). Whether human PSCs have failed to produce chimeras because naïve PSCs in general cannot colonize embryos from distant species or because human PSC are inherently devoid of the attributes of chimeric competence is not known.

To explore this issue, we investigated the differential ability of mESCs, rhesus monkey, and human naïve PSCs to colonize both closely and distantly related host embryos. To circumvent the ban on introducing human embryo-derived PSCs into animal embryos, we used embryo-derived rhesus monkey PSCs and human iPSCs. As a reference, we explored the ability of mESCs, the gold standard of naïve pluripotency, to colonize evolutionary distant host embryos. As host species, we selected rabbit and cynomolgus monkey embryos as hosts. Primates and glires (rodents + lagomorphs) diverged between 85 and 97 million years, while rodents and lagomorphs diverged between 77 and 88 million years (www.timetree.org). The divergence time makes rabbit embryos an almost equidistant environment for comparing the colonizing capabilities of rodent and primate PSCs. In addition, rabbits have several advantages in testing the colonization capacity of human PSCs. The early rabbit embryos share common features with primate embryos in their developmental characteristics (Madeja et al., 2019); unlike the three-dimensional egg-cylinder shape of rodent embryos during gastrulation, primate and rabbit embryos develop into a flattened disc at the surface of the conceptus (Waddington and Waterman, 1933); primate and rabbit embryos are also markedly similar with respect to the timing of zygotic genome activation and the timing and regulation of X-chromosome inactivation (Okamoto et al., 2011). In rodents and primates, gastrulation occurs in the implanted embryo buried within the uterine wall. However, in rabbits, gastrulation begins shortly before implantation, allowing easier access to a wider

developmental window. Furthermore, the rabbit PSC lines derived from pre-implantation embryos require FGF2 and TGFβ for inhibition of differentiation (Wang et al., 2008) and exhibit the cardinal features of primed pluripotency (Osteil et al., 2013, Osteil et al., 2016). Thus, rabbit pre-implantation embryos appear to be more similar to primate embryos than mouse embryos with respect to the mechanisms regulating pluripotency. Therefore, they may be a better host for examining the colonization competence of human PSCs. As a closely related host for Human and rhesus monkey PSCs, we used cynomolgus macaque embryos. The common ancestor of macaques and Humans dates back 29 million years, while rhesus and cynomolgus macaques diverged 3.7 million year ago (www.timetree.org). We explored the differential ability of mESCs, rhesus monkey PSCs and human naïve iPSCs to colonize rabbit and cynomolgus embryos, and drew conclusions on the inherent abilities of rodent and primate naïve PSCs to colonize distantly-related hosts.

Results

Colonization of rabbit embryos by mESCs

Fresh rabbit embryos observed by epifluorescence microscopy typically show a high level of autofluorescence (**Supplemental data S1A**), which could be confounding for the detection of GFP-expressing cells in chimeras. To overcome this limitation, we systematically used an anti-GFP antibody. No immunostaining was observed when applied to rabbit embryos (i) prior to any injection of cells, and (ii) after injection of 10 rhesus wild-type PSCs (LyonES (Wianny et al., 2008)) that do not express any fluorescent reporters. Immunolabeling was observed in both rhesus PSCs expressing GFP as a fusion between tau protein and GFP (LyonES-tauGFP) **(Supplemental data S1B)** and rabbit embryos colonized with naïve-like rabbit iPSCs expressing GFP **(Supplemental data S1C)** (Osteil et al., 2016). Thus, immunolabeling of GFP allows an effective detection of GFP expression in our system.

Mouse ESCs grown in serum/LIF and, specially, in 2i/LIF epitomize naïve pluripotency and, for this reason, we tested their ability to colonize rabbit embryos. For this purpose, 10 mESC-GFP cells cultured in serum/LIF condition were injected into rabbit embryos at the morula stage (E2). The morulas were subsequently cultured for 1–3 days *in vitro* (DIV) and developed into early (E3), mid (E4), and late (E5) blastocysts (1, 2, and 3 DIV, respectively).

The vast majority of rabbit blastocysts had incorporated groups of GFP$^+$ cells (97.5%, n = 81; **Fig. 1A**, **Table S1**). mESCs and their progeny divided very actively, as shown by both the expansion of the GFP$^+$ cell pool during *in vitro* culture of chimeric embryos and a high incorporation of 5-ethylnyl-2'-deoxyuridine (EdU) in most GFP$^+$ cells (**Figs. 1B**, **C**; **Supplemental data S2**). It should be noted that, under the conditions used (very short incorporation time), the EdU labeling of host embryo cells is markedly low. GFP$^+$ cells and their progeny expressed the transcription factors and pluripotency markers Oct4, Nanog and SRY-box transcription factor (Sox)2, as revealed by immunostaining at E5 (3 DIV) (**Figs. 1D, E**). In contrast, GFP$^+$ cells did not express Sox17, a primitive endoderm marker, indicating that they did not differentiate to the primitive endoderm lineage. We performed a similar experiment using cynomolgus monkey embryos as hosts. For this purpose, 10 mESC-GFP cells were injected into cynomolgus embryos at the morula stage (E4). The morulas were subsequently cultured for 3 DIV and developed into mid/late (E7) blastocysts before immunostaining with GFP, Oct4, Nanog, Sox2, and Sox17 antibodies. Among the five embryos analyzed, three contained 8–16 GFP$^+$ cells in the ICM. The first embryo was immunostained with GFP, Oct4, and Sox2 antibodies and contained 16 GFP$^+$/Oct4$^+$/Sox2$^+$ cells. The second one was immunostained with GFP and Nanog antibodies and contained eight GFP$^+$/Nanog$^+$ cells. The third one was immunostained with GFP and Sox17 antibodies and contained eight GFP$^+$/ Sox17$^-$ cells (**Fig. 2**, **Table S1**). In another experiment, mESCs propagated in N2B27 supplemented with LIF, PD0325901, and CHIR99021 (*i.e.*, 2i/LIF condition) were injected into rabbit morulas (10 2i/LIF mESC-GFP cells) and subsequently cultured for 3 DIV prior to immunostaining (**Supplemental data S3A**, **Table S1**). Of the 19 E5 blastocysts obtained, 14 had incorporated groups of GFP$^+$ cells. Immunostaining with Sox2 and Sox17 antibodies showed that 100% of chimeric embryos harbored GFP$^+$ cells expressing Sox2 (n = 7/7), whereas none of them expressed Sox17 (n = 0/7). Overall, these results show that mESCs, whether in serum/LIF or 2i/LIF conditions, continue to express pluripotency markers and expand after injection into evolutionary distant embryos, whether rabbit or cynomolgus monkey embryos.

We subsequently studied the ability of mESCs to colonize the embryonic disk of rabbit pre-gastrula embryos (E6) and the three germ layers after gastrulation (E9). For this purpose, the E2 embryos injected with 10 mESC-GFP cells (grown in serum/LIF) were transferred into the oviducts of surrogate rabbits. Nine embryos were recovered after 4 days (*i.e.*, E6). All contained GFP$^+$ cells expressing Oct4 and Sox2 (**Fig. 1F**, **Supplemental data S3B**, **Table S1**).

Three embryos were immunostained with a Sox17 antibody and did not show Sox17$^+$ cells. On the other hand, the GFP$^+$ cells formed a coherent group of cells in the embryonic disk, suggesting that mouse cells did not mix with rabbit cells. To assess whether mESCs still participated in the development of rabbit embryos after gastrulation, 20 fetuses were recovered 7 days after transfer to surrogate mothers (*i.e.*, E9) (**Supplemental data S3C**, **Table S1**). Fetuses had GFP$^+$/Sox2$^+$, GFP$^+$/Tuj1$^+$ and GFP$^+$/Nanog$^-$ cells in the neurectoderm (n = 12/12). However, they did not have GFP$^+$ cells in embryonic tissues derived from the mesoderm and endoderm. These results strongly suggest that mESCs injected into rabbit morulas contribute to the expansion of the late epiblast until the onset of gastrulation. After gastrulation, mESCs were able to contribute only to the neuroectoderm, but not to other ectodermal structures, or to the mesoderm and endoderm of rabbit gastrula.

Reprogramming rhesus PSCs to naïve pluripotency

The LyonES rhesus line expressing a tauGFP transgene under the control of the ubiquitous CAG promoter has been previously described (Wianny et al., 2008). LyonES-tauGFP cells were infected with the pGAE-STAT3-ER^{T2} lentiviral vector (Chen et al., 2015a), and a clonal cell line stably expressing STAT3-ER^{T2} was isolated as LyonES-tGFP-(S3). Immunostaining with anti-STAT3 antibody showed increased labeling and nuclear translocation following the treatment of LyonES-tGFP-(S3) cells with tamoxifen (**Supplemental data S4A**). LyonES-tGFP-(S3) cells were cultured in the presence of tamoxifen to activate STAT3-ER^{T2} and with 1,000 U/mL of LIF, MEK, and GSK3β inhibitors. Consistent with previous observations in human PSCs (Chen et al., 2015a), the LyonES-tGFP-(S3) cells formed small dome-shaped colonies, which were termed rhesus TL2i (rhTL2i) cells (**Fig. 3A**). These colonies demonstrated identical morphology with that previously described for human TL2i cells (Chen et al., 2015a). We developed a variant of the TL2i protocol, in which MEKi and GSK3βi were replaced by CNIO-47799, a chemical inhibitor of cyclin-dependent kinase (CDK)8 and CDK19 (CDK8/19i) for reprogramming to the naïve state (Lynch et al., In revision). This protocol is referred to as TL−CDK8/19i and the reprogrammed cells as rhesus TL-CDK8/19i (rhTL-CDK8/19i). LyonES-tGFP-(S3) cells were submitted to six other reprogramming protocols previously developed to revert human or monkey PSCs to naïve pluripotency, including NHSM-v and E-NHSM (Gafni et al., 2013, Chen et al., 2015b), 4i/L/b (Fang et al., 2014), t2iLGöY (Takashima et al., 2014, Guo et al., 2016), 5iL/A or 6iL/A (Theunissen et al., 2014), and LCDM (extended pluripotent stem [EPS]) (Yang et

al., 2017b). It should be noted that the six protocols were applied to LyonES-tGFP-S3 cells in the absence of tamoxifen, thus maintaining STAT3-ER^{T2} in an inactive state. LyonES-tGFP-S3 cells differentiated or underwent apoptosis when cultured in LIF/MEKi/GSK3βi (not shown). Of the eight protocols tested, seven (*i.e.,* NHSM-v, E-NHSM, 4i/L/b, t2iLGöY, LCDM [EPS], TL2i, and TL-CDK8/19i) produced rhesus PSCs forming dome-shaped colonies (**Fig. 3A**). Continued instability was observed with protocol 5iL/A, which was subsequently omitted from the study. Unlike conventional rhesus PSCs, which were mechanically passaged in clumps after collagenase dissociation, all reprogrammed cells were routinely single-cell dissociated with trypsin or trypLE. The colonies expressed Oct4 and Sox2 (**Fig. 3A**, **Supplemental data S4B**). They also showed variable expression of naïve transcription factors and cell surface molecules. Notably, transcription factor AP-2 gamma (Tfap2c), Klf4, and transcription factor binding to IGHM enhancer 3 (Tfe3) showed stronger expression after reprogramming with the 4i/L/b, t2iLGöY, TL2i, and TL-CDK8/19i protocols. LCDM (EPS) cells only expressed Klf4 and Tfe3, but not Tfap2c. Cells reprogrammed with the other protocols did not express any of these naïve markers (TFAP2C, KLF4, TFE3). Reconfiguration of the epigenome was observed in TL2i, t2iLGöY, TL-CDK8/19i, and LCDM (EPS) cells, as evidenced by diffuse H3K27me3 immunostaining *vs.* punctate staining in primed, NHSM-v, and E-NHSM cells, reflecting chromatin opening (**Fig. 3A**). Thus, only four cell types, namely, 4i/L/b, t2iLGöY, TL2i, and TL-CDK8/19i, showed all the examined naïve pluripotency markers.

Gene expression was analyzed by bulk RNA sequencing to assess transcriptome reconfiguration in the reprogrammed cells. Principal component analysis (PCA) and hierarchical clustering showed that primed and E-NHSM cells clustered on one side, whereas NHSM-v, 4i/L/b, t2iLGöY, TL2i, and LCDM (EPS) cells clustered on the other side (**Fig. 3B**, **Supplemental data S4C, Table S3**). TL-CDK8/19i cells demonstrated an intermediate position, suggesting that transcriptome reconfiguration was less pronounced. A comparative analysis was performed between the primed and naïve rhesus PSC lines and single-cell RNA-sequencing data of the cynomolgus epiblast (Nakamura et al., 2016). The NHSM-v, 4i/L/b, t2iLGöY, TL2i, and LCDM (EPS) cells also clustered closer to the epiblast cells of the E6/E7 cynomolgus embryo (Nakamura et al., 2016) than the E-NHSM and primed cells (**Fig. 3C**). These results show that, consistent with the immunostaining data, reprogramming of rhesus PSC is characterized by a transcriptome shift reflecting the acquisition of characteristic

features of the pre-implantation epiblast as previously reported with human naïve PSCs (Nakamura et al., 2016).

Premature differentiation of rhesus naïve PSCs after injection into rabbit embryos

The ability of reprogrammed rhesus PSCs to colonize rabbit ICM/epiblast was tested. For this purpose, 10 LyonES-tGFP-(S3) cells of each type [primed, NHSM-v, E-NHSM, LCDM (EPS), 4i/L/b, t2iLGöY, TL2i, and TL-CDK8/19i] were injected into rabbit morulas (E2). The embryos were subsequently cultured for 1–3 DIV and developed into early (E3), mid (E4), and late blastocysts (E5). There was no difference observed in the rate of development between control (uninjected) and injected embryos (not shown). In the first set of experiments, the fate of injected cells was monitored by two-photon microscopy for 48–72 h. Contrary to our observations with mESCs, rhesus PSCs did not actively proliferate in host embryos, and most of them did not incorporate into ICM/epiblast (**Supplemental data S5–S8**). GFP^+ embryos and cell counts confirmed this finding: the number of embryos with GFP^+ cells decreased with time in culture, ranging from 0% (E-NHSM) to 62% (t2iLGöY) at 3 DIV compared with 22–96% at 1 DIV (**Fig. 4A**, **Table S1**). In addition, the percentage of embryos with ≥4 GFP^+ cells diminished in all experimental conditions tested, ranging from 0% (E-NHSM) to 24% (TL2i) at 3 DIV *vs.* 0% (E-NHSM) to 79% (t2iLGöY) at 1 DIV (**Fig. 4B**). These results indicate that rhesus PSCs failed to actively divide and/or were gradually eliminated during embryonic development, regardless of the reprogramming strategy used for conversion to the naïve state. Despite the failure of the rhesus PSCs to thrive in a rabbit embryo environment, variations in the survival rate of GFP^+ cell at 3 DIV were observed between reprogramming strategies. There were no GFP^+ cells observed in embryos injected with either primed rhesus PSCs (0/90) or E-NHSM cells (0/71). In contrast, GFP^+ cells were observed at varying frequencies using other reprogramming protocols. At 3 DIV, the highest rates were observed with TL2i (57%, n = 490), 4i/L/b (41%, n = 228), t2iLGöY (37%, n = 168), LCDM (26%, n = 335), and TL-CDK8/19i (20%, n = 260). TL2i was the only reprogramming method that returned more GFP^+ cells at 2 DIV (58%, n = 145) and 3 DIV (57%, n = 204) compared with 1 DIV (44%, n = 141). These results suggested that TL2i cells have a slightly increased proliferative capacity compared with cells reprogrammed using other methods (**Fig. 4B**).

We subsequently characterized the surviving rhesus PSCs. The chimeric embryos were immunostained with GFP, Oct4, Sox2, Nanog, and Gata6 antibodies at E3 (1 DIV, 335 embryos

with GFP^+ cells, n = 650), E4 (2 DIV, 202 embryos with GFP^+ cells, n = 664), and E5 (3 DIV, 217 embryos with GFP^+ cells, n = 932). $GFP^+/Oct4^+$ and $GFP^+/Gata6^+$ co-immunostaining was frequently observed in chimeric embryos at 3 DIV. In contrast, $GFP^+/Sox2^+$ cells were rarely observed (**Fig. 4C**, **Table S1**). $GFP^+/Sox2^+$, $GFP^+/Nanog^+$, and $GFP^+/Gata6^+$ cells were counted in 754 positive embryos. A strong decrease in the rate of $GFP^+/Sox2^+$ and $GFP^+/Nanog^+$ cells and an increase in the rate of $GFP^+/Gata6^+$ cells were observed between 1 and 3 DIV with all reprogramming protocols (**Fig. 4D**). These results strongly suggest that the vast majority of rhesus PSCs abolished the expression of pluripotency markers and committed prematurely to differentiation after injection into rabbit embryos.

In previous experiments, we compared the colonization capabilities of mESCs and monkey PSCs using the same experimental paradigm, which included single-cell dissociation and embryo culture in 20% O_2 concentration. Rabbit embryos are routinely cultured at atmospheric O_2 concentration (Tapponnier et al., 2017). Thus, we compared the GFP^+ cell colonization rates after culturing host embryos under normoxic (20% O_2) and hypoxic (5% O_2) conditions. Following injection of 10 rhesus TL2i cells, host embryos were cultured under conditions of 5% and 20% O_2 concentration (number of embryos treated: 112 and 109, respectively). The rate of embryos containing GFP^+ cells was lower at 1, 2, and 3 DIV after culture at 5% O_2 concentration (**Supplemental data S9A**). We also evaluated whether microinjection of cell clumps into rabbit embryos would improve the colonization capabilities compared with single-cell suspensions. The experiment was performed using rhesus TL2i cells. At both 1 and 2 DIV, the rate of GFP^+ embryos obtained after injection of small aggregates of 10 cells was lower than that obtained after injection of the same number of isolated cells (1 DIV: 37% *vs.* 53%, respectively; n = 76; 2 DIV: 19% *vs.* 43%, respectively; n = 76; **Supplemental data S9B**). In contrast, at 3 DIV, injection of aggregates of 10 cells yielded slightly better results than those recorded after injection of the same number of isolated cells (18.9% *vs.* 6.25% of GFP^+ embryos, respectively; n = 98). However, we did not observe an increase in the number of GFP^+ cells in the positive embryos. Finally, we evaluated the efficacy of colonization after microinjection of 10 cells into embryos at the morula stage (E2) compared with the blastocyst stage (E4) (**Supplemental data S9C**). At 3 DIV, we observed lower levels of GFP^+ embryos for TL2i cells (39% *vs.* 6%) and 4i/L/b cells (29% *vs.* 0%) after microinjection into blastocyst-stage embryos. On the basis of these additional experiments, we concluded that injection of embryos at the blastocyst stage, Injection of cell clumps, and reduction of O_2

concentration during embryo culture did not improve the rate of embryo colonization by rhesus PSCs.

Previous studies have shown that inhibiting apoptosis either by the addition of the Rock inhibitor Y27632 (Kang et al., 2018), or by overexpression of the anti-apoptotic genes *BCL2* (Masaki et al., 2016) or BMI1 (Huang et al., 2018) enables primed PSCs to colonize host embryos. Therefore, in a final series of microinjections, we asked whether inhibition of apoptosis could improve the engraftment of naïve PSCs into the host embryo. For this purpose, NHSM-v and t2iLGöY PSCs were treated with the ROCK inhibitor Y27632 during dissociation and microinjection into the host embryos. The rates of embryos containing GFP^+ cells were similar at all three time points analyzed (1, 2, and 3 DIV; **Supplemental data S9D**). Thus, addition of Rock inhibitor did not improve the rate of embryo colonization by rhesus naïve PSCs.

Colonization of rabbit and macaque pre-implantation embryos by human PSCs

We subsequently investigated whether human naïve PSCs exhibited a similar behavior to that of rhesus naïve PSCs after injection into rabbit embryos. We tested the colonization capabilities of two human iPSC lines, cR-NCRM2 (Guo et al., 2017), and IR1.7 (Ng et al., 2012), after reprogramming with t2iLGöY (Guo et al., 2017) and TL2i protocols (Chen et al., 2015a), respectively. The cR-NCRM2-t2iLGöY cells express the naïve pluripotency markers TFAP2C, KLF4, KLF17, transcription factor CP2 like 1 (TFCP2L1), and sushi domain containing 2 (SUSD2 (Bredenkamp et al., 2019)), and exhibit diffuse H3K27me3 immunostaining in most cells (H3K27me3) (**Supplemental data S10A**). After injection into rabbit morulas, immuno-fluorescence was used for the detection of human nuclear antigen (HuN) to trace human cells in rabbit host embryos. On days 1, 2, and 3, 93% (n = 29), 65% (n = 31), and 33% (n = 130) of the embryos contained HuN^+ cells in the ICM/epiblast, respectively (**Figs. 5A, B, Table S1**). At 3 DIV, double immunofluorescence analysis showed that 58% (n = 12), 23% (n = 13), and 33% (n = 6) of the embryos had incorporated $HuN^+/SOX2^+$, $HuN^+/NANOG^+$ cells, and $HuN^+/GATA6^+$ cells, respectively. These rates are similar to those previously obtained with t2iLGöY rhesus PSCs (**Fig. 4B**). This suggests that rhesus and human t2iLGöY cells show very similar colonization capabilities after injection into rabbit embryos. Naïve IR1.7-TL2i cells have been described (Chen et al., 2015a) (**Supplemental data S10B**). On days 1, 2, and 3, 85% (n = 39), 50% (n = 36), and 28% (n = 39) of embryos contained HuN^+ cells in the ICM/epiblast,

respectively (**Figs. 5C, D, Table S1**). At 1 DIV, double immunofluorescence analysis showed that 82% (n = 11), 100% (n = 14), and 0.1% (n = 7) of the embryos had incorporated $HuN^+/SOX2^+$, $HuN^+/NANOG^+$ cells, and $HuN^+/GATA6^+$ cells, respectively. At 3 DIV, 0% (n = 6), 0% (n = 4), and 50% (n = 2) of the embryos had incorporated $HuN^+/SOX2^+$, $HuN^+/NANOG^+$ cells, and $HuN^+/GATA6^+$ cells, respectively. These results confirm the results observed with rhesus TL2i cells (**Fig. 4B**), showing a low rate of colonization by $SOX2^+$ human TL2i cells at 3 DIV.

We questioned whether the low rate of proliferation of human TL2i and t2iLGöY cells after injection into rabbit morulas and the low rate of ICM/epiblast colonization were due to the evolutionary distance between the two species. To answer this question, we injected human and rhesus TL2i and human t2iLGöY cells into cynomolgus monkey embryos. Ten cells of each were injected into embryos at the morula stage (E4). The embryos were subsequently cultured for 3 DIV and developed into mid/late (E7) blastocysts before being subjected to triple immunostaining for GFP, OCT4, and NANOG. Of the cynomolgus embryos, 13% (n = 15) had incorporated human GFP^+ t2iLGöY cells, for a total of 5 GFP^+ cells (2 and 3 GFP^+ cells/embryo), of which only 1 was both $OCT4^+$ and $NANOG^+$ (**Fig. 5E**, **Supplemental data S10C**, **Table S1**); 29% (n = 7) of the cynomolgus embryos had incorporated human GFP^+ TL2i cells, for a total of 14 GFP^+ cells (10 and 4 GFP^+ cells/embryo), of which 2 were either $OCT4^+$ or $NANOG^+$ (**Fig. 5F**, **Supplemental data S10C**, **Table S1**); and 29% (n = 7) of cynomolgus embryos had incorporated rhesus TL2i cells, for a total of 3 GFP^+ cells (1 and 2 GFP^+ cells/embryo), none of which were either $Oct4^+$ or $NANOG^+$ (**Supplemental data S10C**, **Table S1**). These results indicate that human iPSCs (IR1.7-TL2i and NCRM2-t2iLGöY) and rhesus monkey PSCs [LyonES-tGFP-(S3)-TL2i] show similarly behaviors after injection into closely and distantly related embryos (cynomolgus and rabbit embryos, respectively).

Cell-cycle distribution and DNA replication of mESCs and rhesus naïve PSCs

To understand why rhesus PSCs stop multiplying when injected into host embryos, we examined both the DNA replication and cell-cycle distribution. We started by examining the incorporation of EdU as a measure of both the fraction of cells that replicate in the cell population (% EdU^+) and the rate of DNA replication (mean EdU incorporation rate) of the cells prior to embryo injection. Measurements were performed in cultured cells ("plated"), after single-cell dissociation with trypsin ("0h"), and after incubation for 1 hour at 37°C ("1h") in order to mimic the conditions encountered by the cells during injection into host embryos.

mESCs incorporate EdU very rapidly (**Fig. 6**), consistent with previous results describing the high rate of 5-bromo-2-deoxyuridine (BrdU) incorporation in mESCs (Savatier et al., 1996). Single-cell dissociation did not alter the percentage of EdU^+ mESCs (77% and 78% of EdU^+ cells in "plated" and "0h" cells, respectively). It slightly decreased in "1h" cells (48% of EdU^+ cells), but the mean rate of EdU incorporation did not vary and even seemed to slightly increase (arbitrary units: 589 and 400 in "0h" and "1 h" cells, respectively, *vs*. 318 in "plated" cells). These observations suggest that DNA replication is not altered by the experimental setting in the vast majority of mESCs. Similar conclusions were made with mESCs cultured in 2i/LIF medium. However, it should be noted that the rate of EdU incorporation was lower under 2i/LIF culture conditions compared with that under serum/LIF conditions. This finding is consistent with those of a previous report showing that mESCs cultured in 2i/LIF exhibit a slower cell cycle compared with their serum/LIF counterparts (Ter Huurne et al., 2017).

The pattern of EdU incorporation in primed LyonES-tGFP-(S3) cells was markedly different. Both the percentage of EdU^+ cells and the mean rate of incorporation were significantly reduced in "plated" cells compared to those measured in mESCs. Both were further reduced in "0h" and "1h" cells. In "1h" cells, DNA replication was almost completely abolished. This reveals the inherent failure of primed LyonES-tGFP-(S3) cells to sustain cell cycle progression following single-cell dissociation. Interestingly, reprogramming primed LyonES-tGFP-(S3) cells with 4i/L/b, TL2i and t2iLGöY protocols significantly increased both the percentage of EdU^+ cells and the mean incorporation rate, consistent with a previous report indicating that resetting naïve-like features accelerated the cell cycle of human PSCs (Chen et al., 2015a). However, unlike mESCs, rhesus naïve 4i/L/b, TL2i and t2iLGöY cells slowed DNA replication after dissociation, evidenced by a significant reduction of EdU incorporation in both "0h" and "1h" cells. In "1h" cells, only 6%, 10%, and 18% of the 4i/L/b, TL2i and t2iLGöY cells, respectively, incorporated EdU (compared to 48% of mESCs in the same experimental condition). Furthermore, the mean rate of incorporation was considerably reduced as compared to "plated" 4i/L/b, TL2i and t2iLGöY cells and "1h" control mESCs. Overall, these results indicate that rhesus naïve PSCs, unlike mESCs, fail to maintain active DNA replication in this experimental setting. This suggests that the vast majority of naive rhesus cells are markedly slowed down in their mitotic cycle at the time they are injected into host embryos.

Rhesus PSCs stall in the G1 phase after transfer into rabbit embryos

We observed that mESCs continue to actively replicate their DNA after injection into rabbit embryos and colonization of the ICM/epiblast (**Fig. 1C**). Therefore, we investigated whether naïve rhesus cells that survive injection and successfully colonize the ICM/epiblast retain a high proliferative capacity. For this purpose, 10 rhesus TL2i cells were injected into rabbit embryos at the morula stage. The embryos were subsequently cultured for 1 and 2 DIV prior to pulse-labeling with EdU. At 1 DIV, seven embryos had GFP^+ cells in the ICM/epiblast (37%, n = 19) for a total of 29 GFP^+ cells. Triple immunostaining for GFP, Sox2, and EdU showed that 24 (82%) of these 29 GFP^+ cells expressed Sox2, of which only four have incorporated EdU (**Supplemental data S11**). At 2 DIV, nine embryos had GFP^+ cells in the ICM/epiblast (60%, n = 15) for a total of 61 GFP^+ cells. Of these 61 GFP^+ cells, 44 (72%) expressed Sox2, and 1 incorporated EdU (2%). These results reveal that the rhesus naïve cells that survived and colonized the rabbit embryos retarded their DNA replication and potentially underwent growth arrest.

To obtain further insight into the cell cycle of the mESCs and rhesus 4i/L/b, TL2i, and t2ILGöY naïve PSCs after injection into rabbit embryos, we generated cell lines expressing the FUCCI(CA) reporter system (Sakaue-Sawano et al., 2017). The mESCs expressing *PB-Puro^R-CAG-mVenus:hGeminin-IRES-mCherry:hCdt1*, hereinafter referred to as mESC-FUCCI(CA), exhibited a cell cycle distribution typical of mESCs (18%, 69%, and 11% of cells in G1, S, and G2 phases, respectively; **Supplemental data S12A, B**). On the other hand, rhesus PSC-FUCCI(CA) cells exhibited an extended G1 phase relative to other cell cycle phases (43%, 36%, and 13% of the cells in G1, S, and G2 phases, respectively) (**Supplemental data S12C, D**). After injection into rabbit embryos, mESC-FUCCI(CA) cells proliferated actively during the 3 DIV, as shown by the expansion of the $mVenus^+$ cell population identified through immunostaining with an anti-mVenus antibody (green) in 100% of the embryos (**Figs. 7A, B**). Even after 3 DIV, $mCherry^+$ cells (red), identified using an anti-mCherry antibody, and $mVenus^+/mCherry^+$ cells (yellow) were proportionally less numerous, indicating that only rare mESCs were in G1 and G2 phases, respectively. In addition, at all time-points analyzed, there were no embryos containing only $mCherry^+$ (red) cells (n = 27) (**Fig. 7B**). These results indicate that mESCs continue to proliferate actively for at least three days after injection into host embryos, in line with the EdU incorporation data.

On the other hand, the cell cycle distribution of rhesus PSC-FUCCI(CA) cells after injection into rabbit embryos was clearly different, regardless of the method used (4i/L/b, TL2i, and t2iLGöY) for reprogramming to the naïve state. At 1 DIV, the majority of embryos contained only mCherry$^+$ (red) cells (t2iLGöY, 60%, n = 47; TL2i, 68%, n = 11; 4i/L/b, 60%, n = 25). The remaining embryos contained both mVenus$^+$ (green) and mVenus$^+$/mCherry$^+$ (yellow) cells in addition to mCherry$^+$ (red) cells. In embryos injected with TL2i and 4i/L/b cells, the rate of embryos containing only mCherry$^+$ (red) cells increased over time in culture, reaching 78% (n = 9) and 100% (n = 3) with 4i/L/b and TL2i cells, respectively, at 3 DIV (**Fig. 7B**). In embryos injected with t2iLGöY cells, the proportion of embryos containing only mCherry$^+$ (red) cells first decreased at 2 DIV (35%, n = 36) and subsequently increased at 3 DIV (95%, n = 35) **(Fig. 7B)**. These results indicate that naïve rhesus PSC-FUCCI(CA) cells accumulate in the G1 phase of the cell cycle after injection into rabbit embryos.

Discussion

In our study, we aimed to understand why human naïve PSCs failed to colonize mouse and pig embryos (Masaki et al., 2015, Theunissen et al., 2016, Wu et al., 2017), despite exhibiting characteristic features of naïve pluripotency as primarily defined in rodents. Our main conclusion is that human and NHP naïve PSCs are inherently unfit to remain mitotically active during embryo colonization and therefore differentiate prematurely.

The first question we addressed was whether or not host embryos are permissive to colonization by naive PSCs. To answer this question, we injected mouse ESCs into rabbit and cynomolgus embryos and showed that they continue to express pluripotency markers, they remain mitotically active for at least 3 days *in vitro*, and they contributed to the expansion of the host epiblast. Some of them contributed to the formation of the neural tube in rabbit post-implantation embryos. We conclude that the ICM and epiblast of rabbit and cynomolgus embryos are permissive to colonization by bona fide naïve PSCs. These results may seem to contradict those of Wu *et al.* who injected mouse ESCs into pig embryos and observed no chimerism at d21-d28 of gestation (Wu et al., 2017). Differentiated cells derived from mouse ESCs are likely to disappear from the chimera through cell competition in later stages of

development, however, this should not obscure the fact that the mouse ESCs are initially capable of colonizing pre-implantation embryos very efficiently.

In sharp contrast with mESCs, none of the naïve rhesus and human PSCs tested in the same experimental paradigm is capable of massively colonizing the ICM and epiblast of the host, whether rabbit or cynomolgus monkey embryos. Some cells retaining the expression of pluripotency markers were observed at 3 DIV in rabbit embryos after injection of LCDM (EPS) (9% of total embryos), 4i/L/b (2% of total embryos), TL2i (5% of total embryos), TL-CDK8/19i (2% of total embryos), and t2iLGöY PSCs (3% of total embryos) (Table 1). In these 234 chimeric embryos, the total number of GFP^+ cells expressing pluripotency markers after 3 DIV was 3.26 +/- 1.27, when 10 cells were injected at the morula stage. The other cells differentiated prematurely. In contrast, up to 40 $GFP^+/NANOG^+$ and 36 $GFP^+/SOX2^+$ cells/embryo were observed following injection of 10 mESCs into rabbit morulas after the same period of culture. Similarly, up to 23 $GFP^+/SOX2^+$ cells/embryo were observed after injection of mESC-2i/LIF. These results illustrate the striking difference observed between mouse ESCs and primate PSCs in the stability of pluripotency gene expression after injection into host embryos. As a result, none of the protocols tested confer an embryo colonization competence to primate naïve PSCs similar to that of mESCs. It should be noted however that the different protocols tested for reprogramming human and NHP PSCs did not yield identical results. We were unable to generate undeniable chimeric blastocysts with the E-NHSM and NHSM-v protocols. This result is in contradiction with a previous publication reporting efficient colonization of cynomolgus monkey embryos by PSCs reprogrammed using the NHSM-v protocol (Chen et al., 2015b). This difference can be explained by the immunodetection of GFP^+ cells in the developing embryos, which eliminates the confounding effect of autofluorescence due to dying and necrotic cells. We did not observe significant differences in the rate of colonization by $GFP^+/NANOG^+$, $GFP^+/Oct4^+$, and $SOX2^+/GFP^+$ cells between the other five reprogramming protocols. We do not rule out the possibility that some of these protocols may be more effective than others in generating cells capable of colonization. However, the number of unquestionable chimeric blastocysts obtained with each of these protocols was insufficient to conclude about significant differences.

After injection into rabbit and macaque monkey morulas, most rhesus and human naïve PSCs undergo cell death. We showed that the few cells that survive after 3 DIV stall in the G1 phase and commit to differentiation evidenced by the loss of pluripotency markers

(OCT4, SOX2 and NANOG) and the activation of differentiation markers (GATA6 and SOX17). This is in sharp contrast with mESCs, which continue to actively proliferate after injection into host embryos. These results reveal the inability of human and rhesus monkey naïve PSCs to remain mitotically active in an unfavorable environment and question their very nature. Despite requiring complex culture media, human and NHP naïve PSCs self-renew in a more precarious equilibrium than mESCs. This suggests a much higher sensitivity to alterations of their local environment, possibly explaining the poor performance of human and rhesus monkey naïve PSCs in colonizing the epiblast of host embryos. As a matter of fact, disruption of the rhesus PSC cell cycle is already evidenced immediately after the colony dissociation (i.e. prior to embryo injection) where most rhesus naïve PSCs cells undergo a drastic slowdown in DNA replication. We speculate that only few cells (<< 1 in 10) retain the capacity to actively divide and re-enter the next division cycle when introduced into the embryo environment.

In the prospect of generating interspecies chimeras, an equally important issue is the influence of the host species on the rate of colonization. Rhesus and human PSCs (TL2i and t2iLGöY reprogramming protocols) did not show a marked difference in survival rate and stability of pluripotency gene expression after injection into rabbit and cynomolgus embryos. This strongly suggests that the relative phylogenetic distance between the donor cells and host species has limited or no influence on the outcome of injection during pre-implantation development. It also suggests that rabbit embryos are a valid model system to explore further improvements.

Materials and Methods

A detailed description of the procedures is provided in Supplemental Experimental Procedures.

Cell lines, media composition, and culture

Primed to naïve conversion was performed using previously described protocols, including E-NHSM (https://hannalabweb.weizmann.ac.il) (Gafni et al., 2013), NHSM-v (Chen et al., 2015b), 4i/L/b (Fang et al., 2014), 5iL/A (Theunissen et al., 2014), t2iLGoY (Guo et al., 2017), TL2i (Chen et al., 2015a), TL-CDK8/19i [modified from (Lynch et al., In revision)], and LCDM

(EPS) (Yang et al., 2017a). Detailed protocols are provided in Supplemental experimental procedure.

Generation of rhesus and cynomolgus monkey embryos and cell microinjection

Macaque cynomolgus embryos were produced through ovarian stimulation, followed by intra-cytoplasmic sperm injection (ICSI) of oocytes, as previously described (Tachibana et al., 2012). Briefly, females received twice-daily injections of 25 IU of recombinant human follicle-stimulating hormone (MSD laboratories) from days 1 to 8 (starting at day 1–4 of the menstrual cycle). They received 30 IU of recombinant human luteinizing hormone (Merck) on days 7 and 8. Females received an injection of gonadotropin-releasing hormone antagonist (MSD laboratories) (0.075 mg/kg body weight) on day 8, and an injection of 1,040 IU of human chorionic gonadotropin (Merck) at day 8. Estradiol, luteinizing hormone, progesterone dosage, and ultrasonographic scans were performed to monitor ovarian response. Follicle aspiration and oocyte retrieval were performed by laparoscopy 36 h after injection of human chorionic gonadotropin. Oocytes were transferred to HEPES-buffered TALP medium containing 3 mg/mL of bovine serum albumin (Sigma). Cumulus and granulosa cells were removed by incubating the oocytes for 30 s with hyaluronidase (300 µg/mL). Metaphase II stage oocytes were selected for ICSI and transferred to drops of hamster embryo culture medium-9 (HECM9) covered by liquid paraffin (Origio) at 37 °C in a 5% O_2 + 5% CO_2 atmosphere. Four days after fertilization (E4), morula-stage embryos were microinjected with 10 cells and further cultured in drops of PSC medium for 4 h. PSC media were those used for culturing the cells prior to injection, depending on the reprogramming protocols. After 4 h, embryos were transferred into a 1:1 mix of PSC medium and HECM9 and further cultured for 20 h. After 24 h, embryos were transferred to HECM9 and further cultured.

Production of rabbit embryos, cell microinjection, embryo culture, and transfer

Rabbit embryos were produced by ovarian stimulation. Briefly, sexually mature New Zealand white rabbits were injected with follicle-stimulating hormone and gonadotropin-releasing hormone, followed by artificial insemination or breeding, as previously described. Eight-cell-stage embryos (E1.5) were flushed from explanted oviducts 36–40 h after insemination and cultured in a 1:1:1 mixture of RPMI 1640 medium, DMEM, and Ham's F10 (RDH medium; Thermo Fisher Scientific) at 38 °C in 5% CO_2 until cell microinjection. For the latter procedure,

10 cells were microinjected under the zona pellucida of morula (E2.5)- or blastocyst (E4)-stage rabbit embryos. The embryos were further cultured using the same experimental procedure as for monkey embryo. For embryo transfer, surrogate mothers were prepared through intramuscular injection of 1.6 µg of buserelin acetate (Intervet). Morula-stage embryos (6–8) were transferred to each oviduct of the recipient by laparoscopy. Four days after transfer, pre-implantation embryos (E6) were recovered by flushing the explanted uterine horns. Post-implantation-stage embryos (E9) were recovered by dissecting the uterine horns.

RNA sequencing

RNA from cell lines was extracted from 4–5.10^6 cells using the RNeasy mini-kit (Qiagen). The libraries were prepared using 200 ng of RNA with the NextFlex Rapid Directional mRNA-Seq kit (Bioo-Scientific). Samples were sequenced on a NextSeq500 sequencing machine (Illumina) as single reads of 75 bp. The bcl2fastq conversion software was used for demultiplexing (Illumina), and data trimming was performed using Cutadapt. The sequencing depth for each sample was approximately 30 million reads, which were subsequently mapped to the Mmul8 rhesus macaque genome using the HISAT2 alignment program and quantified with the HTseq script.

Data availability

The RNA-Seq datasets generated during this study are available under GEO accession number: GSE146178.

Ethics

All procedures in macaque monkeys were approved by the French ethics committee CELYNE (approval number: APAFIS#4858). All animal procedures in rabbits were approved by the French ethics committee CELYNE (APAFIS#6438). Chimera experiments involving human iPSCs were approved by the INSERM ethics committee.

Acknowledgments

We are grateful to all members of the animal facility team for their work and dedication. We thank Dr. Austin Smith for sharing the cR-NCRM2 cell line and RIKEN BRC DNABank for providing the mCherry-hCdt1(1/100)Cy(-)/pcDNA3 and mVenus-hGeminin(1/110)/pcDNA3 plasmids. This work was supported by the Fondation pour la Recherche Medicale (DEQ20170336757 and ARF20140129246), The fondation pour la recherche contre le cancer (RAC18005CCA), the Infrastructure Nationale en Biologie et Santé INGESTEM (ANR-11-INBS-0009), the IHU-B CESAME (ANR-10-IBHU-003), the LabEx REVIVE (ANR-10-LABX-73), the LabEx "DEVweCAN" (ANR-10-LABX-0061), the LabEx "CORTEX" (ANR-11-LABX-0042), and the University of Lyon within the program "Investissements d'Avenir"(ANR-11-IDEX-0007). Work in the laboratory of M.S. was funded by the IRB and by grants from the Spanish Ministry of Economy co-funded by the European Regional Development Fund (ERDF) (SAF2017-82613-R), the European Research Council (ERC-2014-AdG/669622) and "La Caixa" Foundation.

Authors' contribution

I.A., C.R., A.M., E.M., V.C., A.B-M., N.D., F.W., and M.A. performed cell and embryo cultures and cell characterizations.

M.D. and T.J. performed animal surgery.

G.M., C.M., and O.R. performed bioinformatic analyses.

C.L., M.S., and C.D. shared unpublished expertise.

I.A. and P.S. analyzed the data and wrote the manuscript.

Declaration of interest

The authors declare no competing interest.

Figure legends

Figure 1: Colonization of rabbit embryos by mouse ESCs (mESCs). (**A**) Epifluorescence images of the early- (E3, 1 DIV) and mid-blastocyst-stage rabbit embryos (E4, 2 DIV) resulting from microinjection of 10 mESC-GFP cells (scale bars: 50 µm). (**B**) Two-photon microscope images of the late blastocyst-stage rabbit embryos (E2–E5, 0–3 DIV) resulting from microinjection of 10 mESC-GFP cells (scale bar: 50 µm). (**C**) Immunostaining of GFP and EdU in a late blastocyst-stage rabbit embryo (E5, 3 DIV) after microinjection of 10 mESC-GFP cells into the morula-stage (E2) embryo (confocal imaging; scale bars: 50 µm). (**D**) Immunostaining of GFP, Oct4, Sox2, Nanog, and Sox17 of late blastocyst-stage rabbit embryos (E5, 3 DIV) after microinjection of 10 mESC-GFP cells into morula-stage (E2) embryos (confocal imaging; scale bars: 50 µm) (n = 135). (**E**) Histogram of percentage of rabbit embryos with $GFP^+/Oct4^+$, $GFP^+/Sox2^+$, $GFP^+/Nanog^+$, and $GFP^+/Sox17^+$ cells at 3 DIV (n = 74). (**F**) Immunostaining of GFP, Oct4, and Sox2 in rabbit embryos at the pre-gastrula stage (E6) after microinjection of mESC-GFP cells into morula-stage (E2) embryos and transfer to a surrogate mother (confocal imaging; scale bars: 50 µm) (n = 9).

Figure 2: Colonization of cynomolgus embryos by mouse ESCs (mESCs). Immunostaining of GFP, Oct4, Sox2, and Sox17 of late blastocyst-stage (E7) cynomolgus embryos after microinjection of 10 mESC-GFP cells into morula-stage (E4) embryos (confocal imaging; scale bars: 50 µm) (n = 7).

Figure 3: Characterization of rhesus PSCs after reprogramming to naïve pluripotency. (**A**) Phase contrast and immunostaining of Oct4, Sox2, Tfap2c, Klf4, Tfe3, and H3K27me3 in LyonES-tGFP-(S3) cells, before (primed rhPSCs) and after reprogramming to the naïve state (E-NHSM, NHSM-v, 4i/L/b, TL2i, t2iLGöY, LCDM (EPS), and TL-CDK8/19i) (confocal imaging; scale bars: 50 µm). (**B**) Principal component analysis (PCA) for primed PSCs, E-NHSM, NHSM-v, 4i/L/b, TL2i, t2iLGöY, LCDM, and TL-CDK8/19i populations based on RNA-sequencing data. (**C**) PCA for primed PSCs, E-NHSM, NHSM-v, 4i/L/b, TL2i, t2iLGöY, LCDM, and TL-CDK8/19i populations based on bulk RNA-seq and single-cell RNA-seq data of cynomolgus epiblast from E6 to E9 embryos (Nakamura et al., 2016).

Figure 4: Competence of rhesus naïve PSCs to colonize rabbit embryos. (**A**) Percentage of rabbit embryos with GFP$^+$ cells, 1–3 days (1–3 DIV) after injection of rhesus LyonES-tGFP-(S3) cells into morula-stage (E2) embryos, before (Primed) and after reprogramming to the naïve state (E-NHSM, NHSM-v, 4i/L/b, TL2i, t2iLGöY, LCDM (EPS), and TL-CDK8/19i) (n = 650 at 1 DIV; n = 664 at 2 DIV; n = 932 at 3 DIV). (**B**) Percentage of rabbit embryos with 0, 1, 2, 3, or >3 GFP$^+$ cells 1–3 days (1–3 DIV) after injection of rhesus LyonES-tGFP-(S3) cells into morula-stage (E2) embryos (n = 650 at 1 DIV; n = 664 at 2 DIV; n = 932 at 3 DIV). (**C**) Immunostaining of GFP, Oct4, Sox2, and Gata6 in late blastocyst-stage (E5) rabbit embryos after microinjection of rhesus PSCs (confocal imaging; scale bars: 50 µm). (**D**) Percentage of GFP$^+$/Nanog$^+$, GFP$^+$/Sox2$^+$, and GFP$^+$/Gata6$^+$ cells in rabbit embryos 1–3 days after injection of rhesus PSCs (n = 232).

Figure 5: Colonization of rabbit and cynomolgus embryos by human iPSCs. (**A**) Immunostaining of HuN, SOX2, NANOG, and GATA6 in late blastocyst-stage rabbit embryos (E5, 3 DIV) after microinjection of NCRM2-t2iLGöY cells into morula-stage (E2) embryos (confocal imaging; scale bars: 50 µm). (**B**) Left: Percentage of rabbit embryos with 0, 1, 2, 3, or >3 GFP$^+$ cells at 1–3 days (1–3 DIV) after injection of NCRM2-t2iLGöY cells (n = 191). Right: Percentage of rabbit embryos with HuN$^+$/SOX2$^+$, HuN$^+$/NANOG$^+$, and HuN$^+$/GATA6$^+$ cells at 3 DIV (n = 130). (**C**) Immunostaining of HuN, SOX2, NANOG, and GATA6 in late blastocyst-stage rabbit embryos (E5, 3 DIV) after microinjection of IR7.1-TL2i cells into morula-stage (E2) embryos (confocal imaging; scale bars: 50 µm). (**D**) Left: Percentage of rabbit embryos with 0, 1, 2, 3, or >3 GFP$^+$ cells at 1–3 days (1–3 DIV) after injection of IR7.1-TL2i cells (n = 114). Right: Percentage of rabbit embryos with HuN$^+$/SOX2$^+$, HuN$^+$/NANOG$^+$, and HuN$^+$/GATA6$^+$ cells at 3 DIV (n = 115). **(E)** Immunolabeling of GFP, OCT4, and NANOG in late blastocyst-stage cynomolgus embryos (E7) after microinjection of human NCRM2-t2iLGöY cells. **(F)** Immunolabeling of GFP, OCT4, and NANOG in late blastocyst-stage cynomolgus embryos (E7) after microinjection of human IR7.1-TL2i cells (confocal imaging; scale bars: 50 µm) (n = 29).

Figure 6: Incorporation of EdU into mouse ESCs and rhesus PSCs before and after reprogramming to the naïve state. Flow cytometry analysis of EdU incorporation and propidium iodide (PI) staining of mouse ESCs (serum/LIF and 2i/LIF) and rhesus PSCs (primed,

4i/L/b, TL2i, and t2iLGöY) in “plated”, “0h”, and “1h” condition. Numbers indicate percentages of EdU^+ cells/mean rate of incorporation (arbitrary units).

Figure 7: Cell cycle distribution of mouse and rhesus PSCs after injection into rabbit embryos. (**A**) Phase contrast and epifluorescence imaging of mouse ESCs and rhesus TL2i, 4i/L/b, and t2iLGöY PSCs expressing the FUCCI(CA) cell cycle reporter system. Immunostaining of mVenus and mCherry in rabbit embryos 1–3 days (1–3 DIV) after microinjection of FUCCI(CA) mouse and rhesus PSCs into morula-stage (E2) embryos (confocal imaging, scale bars: 50 µm). **(B)** Histogram of the percentage of rabbit embryos having cells in G1, S, and G2 phase of the cell cycle at 1, 2, and 3 DIV (n = 220).

Supplemental data movie legends

Movie S2: Two-photon microscopy analysis of mESC-GFP cells after microinjection into a rabbit embryo (E2) and follow-up for 48–72 h.

Movie S5: Two-photon microscopy analysis of rhesus 4i/L/b PSCs after microinjection into a rabbit embryo (E2) and follow-up for 48–72 h.

Movie S6: Two-photon microscopy analysis of rhesus t2iLGöY PSCs after microinjection into a rabbit embryo (E2) and follow-up for 48–72 h.

Movie S7: Two-photon microscopy analysis of Rhesus TL2i PSCs after microinjection into a rabbit embryo (E2) and follow-up for 48–72 h.

Movie S9: Two-photon microscopy analysis of Rhesus E-NHSM PSCs after microinjection into a rabbit embryo (E2) and follow-up for 48–72 h.

References

BREDENKAMP, N., STIRPARO, G. G., NICHOLS, J., SMITH, A. & GUO, G. 2019. The Cell-Surface Marker Sushi Containing Domain 2 Facilitates Establishment of Human Naive Pluripotent Stem Cells. *Stem Cell Reports,* 12**,** 1212-1222.

CHAN, Y. S., GOKE, J., NG, J. H., LU, X., GONZALES, K. A., TAN, C. P., TNG, W. Q., HONG, Z. Z., LIM, Y. S. & NG, H. H. 2013. Induction of a human pluripotent state with distinct regulatory circuitry that resembles preimplantation epiblast. *Cell Stem Cell,* 13**,** 663-75.

CHEN, H., AKSOY, I., GONNOT, F., OSTEIL, P., AUBRY, M., HAMELA, C., ROGNARD, C., HOCHARD, A., VOISIN, S., FONTAINE, E., MURE, M., AFANASSIEFF, M., CLEROUX, E., GUIBERT, S., CHEN, J., VALLOT, C., ACLOQUE, H., GENTHON, C., DONNADIEU, C., DE VOS, J., SANLAVILLE, D., GUÉRIN, J.-F., WEBER, M., STANTON, L. W., ROUGEULLE, C., PAIN, B., BOURILLOT, P. & SAVATIER, P. 2015a. Reinforcement of STAT3 activity reprogrammes human embryonic stem cells to naïve-like pluripotency. *Nat Commun,* 6**,** 7095-7112.

CHEN, Y. & LAI, D. 2014. Pluripotent States of Human Embryonic Stem Cells. *Cell Reprogram,* 17**,** 1-6.

CHEN, Y., NIU, Y., LI, Y., AI, Z., KANG, Y., SHI, H., XIANG, Z., YANG, Z., TAN, T., SI, W., LI, W., XIA, X., ZHOU, Q., JI, W. & LI, T. 2015b. Generation of Cynomolgus Monkey Chimeric Fetuses using Embryonic Stem Cells. *Cell Stem Cell,* 17**,** 116-124.

COLLIER, A. J. & RUGG-GUNN, P. J. 2018. Identifying Human Naive Pluripotent Stem Cells - Evaluating State-Specific Reporter Lines and Cell-Surface Markers. *Bioessays***,** e1700239.

DAVIDSON, K. C., MASON, E. A. & PERA, M. F. 2015. The pluripotent state in mouse and human. *Development,* 142**,** 3090-9.

FANG, R., LIU, K., ZHAO, Y., LI, H., ZHU, D., DU, Y., XIANG, C., LI, X., LIU, H., MIAO, Z., ZHANG, X., SHI, Y., YANG, W., XU, J. & DENG, H. 2014. Generation of naive induced pluripotent stem cells from rhesus monkey fibroblasts. *Cell Stem Cell,* 15**,** 488-96.

GAFNI, O., WEINBERGER, L., MANSOUR, A. A., MANOR, Y. S., CHOMSKY, E., BEN-YOSEF, D., KALMA, Y., VIUKOV, S., MAZA, I., ZVIRAN, A., RAIS, Y., SHIPONY, Z., MUKAMEL, Z., KRUPALNIK, V., ZERBIB, M., GEULA, S., CASPI, I., SCHNEIR, D., SHWARTZ, T., GILAD, S., AMANN-ZALCENSTEIN, D., BENJAMIN, S., AMIT, I., TANAY, A., MASSARWA, R., NOVERSHTERN, N. & HANNA, J. H. 2013. Derivation of novel human ground state naive pluripotent stem cells. *Nature,* 504**,** 282-286.

GUO, G., VON MEYENN, F., ROSTOVSKAYA, M., CLARKE, J., DIETMANN, S., BAKER, D., SAHAKYAN, A., MYERS, S., BERTONE, P., REIK, W., PLATH, K. & SMITH, A. 2017. Epigenetic resetting of human pluripotency. *Development,* 144**,** 2748-2763.

GUO, G., VON MEYENN, F., SANTOS, F., CHEN, Y., REIK, W., BERTONE, P., SMITH, A. & NICHOLS, J. 2016. Naive Pluripotent Stem Cells Derived Directly from Isolated Cells of the Human Inner Cell Mass. *Stem Cell Reports,* 6**,** 437-446.

HUANG, K., MARUYAMA, T. & FAN, G. 2014. The naive state of human pluripotent stem cells: a synthesis of stem cell and preimplantation embryo transcriptome analyses. *Cell Stem Cell,* 15**,** 410-5.

HUANG, K., ZHU, Y., MA, Y., ZHAO, B., FAN, N., LI, Y., SONG, H., CHU, S., OUYANG, Z., ZHANG, Q., XING, Q., LAI, C., LI, N., ZHANG, T., GU, J., KANG, B., SHAN,

Y., LAI, K., HUANG, W., MAI, Y., WANG, Q., LI, J., LIN, A., ZHANG, Y., ZHONG, X., LIAO, B., LAI, L., CHEN, J., PEI, D. & PAN, G. 2018. BMI1 enables interspecies chimerism with human pluripotent stem cells. *Nat Commun,* 9**,** 4649.

KANG, Y., AI, Z., DUAN, K., SI, C., WANG, Y., ZHENG, Y., HE, J., YIN, Y., ZHAO, S., NIU, B., ZHU, X., LIU, L., XIANG, L., ZHANG, L., NIU, Y., JI, W. & LI, T. 2018. Improving Cell Survival in Injected Embryos Allows Primed Pluripotent Stem Cells to Generate Chimeric Cynomolgus Monkeys. *Cell Rep,* 25**,** 2563-2576 e9.

LI, M. & IZPISUA BELMONTE, J. C. 2018. Deconstructing the pluripotency gene regulatory network. *Nat Cell Biol,* 20**,** 382-392.

LYNCH, C. J., BERNAD, R., MARTINEZ-VAL, A., SHAHBAZI, M., NOBREGA-PEREIRA, S., CALVO, I., BLANCO, C., RICHART-GINES, L., GRANA-CASTRO, O., GOMEZ-LOPEZ, G., ORTEGA, S., AKSOY, I., PRIETO, S., FERNANDEZ, A. F., SIERRA ZAPICO, M. I., FRAGA, M., PASTOR, J., SAVATIER, P., FISHER, D., MUNOZ, J., ZERNICKA-GOETZ, M. & SERRANO, M. Global hyperactivation of enhancers stabilizes human and mouse naïve pluripotency. *Nat Cell Biol* (In revision)

MADEJA, Z. E., PAWLAK, P. & PILISZEK, A. 2019. Beyond the mouse: non-rodent animal models for study of early mammalian development and biomedical research. *Int J Dev Biol,* 63**,** 187-201.

MASAKI, H., KATO-ITOH, M., TAKAHASHI, Y., UMINO, A., SATO, H., ITO, K., YANAGIDA, A., NISHIMURA, T., YAMAGUCHI, T., HIRABAYASHI, M., ERA, T., LOH, K. M., WU, S. M., WEISSMAN, I. L. & NAKAUCHI, H. 2016. Inhibition of Apoptosis Overcomes Stage-Related Compatibility Barriers to Chimera Formation in Mouse Embryos. *Cell Stem Cell,* 19**,** 587-592.

MASAKI, H., KATO-ITOH, M., UMINO, A., SATO, H., HAMANAKA, S., KOBAYASHI, T., YAMAGUCHI, T., NISHIMURA, K., OHTAKA, M., NAKANISHI, M. & NAKAUCHI, H. 2015. Interspecific in vitro assay for the chimera-forming ability of human pluripotent stem cells. *Development,* 142**,** 3222-3230.

NAKAMURA, T., OKAMOTO, I., SASAKI, K., YABUTA, Y., IWATANI, C., TSUCHIYA, H., SEITA, Y., NAKAMURA, S., YAMAMOTO, T. & SAITOU, M. 2016. A developmental coordinate of pluripotency among mice, monkeys and humans. *Nature,* 537**,** 57-62.

NG, S. Y., JOHNSON, R. & STANTON, L. W. 2012. Human long non-coding RNAs promote pluripotency and neuronal differentiation by association with chromatin modifiers and transcription factors. *EMBO J,* 31**,** 522-33.

NICHOLS, J. & SMITH, A. 2009. Naive and primed pluripotent states. *Cell Stem Cell,* 4**,** 487-92.

OKAMOTO, I., PATRAT, C., THEPOT, D., PEYNOT, N., FAUQUE, P., DANIEL, N., DIABANGOUAYA, P., WOLF, J. P., RENARD, J. P., DURANTHON, V. & HEARD, E. 2011. Eutherian mammals use diverse strategies to initiate X-chromosome inactivation during development. *Nature,* 472**,** 370-4.

OSTEIL, P., MOULIN, A., SANTAMARIA, C., JOLY, T., JOUNEAU, L., AUBRY, M., TAPPONNIER, Y., ARCHILLA, C., SCHMALTZ-PANNEAU, B., LECARDONNEL, J., BARASC, H., MOUNEY-BONNET, N., GENTHON, C., ROULET, A., DONNADIEU, C., ACLOQUE, H., GOCZA, E., DURANTHON, V., AFANASSIEFF, M. & SAVATIER, P. 2016. A Panel of Embryonic Stem Cell Lines Reveals the Variety and Dynamic of Pluripotent States in Rabbits. *Stem Cell Reports,* 7**,** 383-398.

OSTEIL, P., TAPPONNIER, Y., MARKOSSIAN, S., GODET, M., SCHMALTZ-PANNEAU, B., JOUNEAU, L., CABAU, C., JOLY, T., BLACHERE, T., GOCZA, E., BERNAT, A., YERLE, M., ACLOQUE, H., HIDOT, S., BOSZE, Z., DURANTHON, V.,

SAVATIER, P. & AFANASSIEFF, M. 2013. Induced pluripotent stem cells derived from rabbits exhibit some characteristics of naive pluripotency. *Biol Open,* 2**,** 613-28.

SAKAUE-SAWANO, A., YO, M., KOMATSU, N., HIRATSUKA, T., KOGURE, T., HOSHIDA, T., GOSHIMA, N., MATSUDA, M., MIYOSHI, H. & MIYAWAKI, A. 2017. Genetically Encoded Tools for Optical Dissection of the Mammalian Cell Cycle. *Mol Cell,* 68**,** 626-640 e5.

SAVATIER, P., LAPILLONNE, H., VAN GRUNSVEN, L. A., RUDKIN, B. B. & SAMARUT, J. 1996. Withdrawal of differentiation inhibitory activity/leukemia inhibitory factor up-regulates D-type cyclins and cyclin-dependent kinase inhibitors in mouse embryonic stem cells. *Oncogene,* 12**,** 309-22.

TACHIBANA, M., SPARMAN, M., RAMSEY, C., MA, H., LEE, H. S., PENEDO, M. C. & MITALIPOV, S. 2012. Generation of Chimeric Rhesus Monkeys. *Cell,* 148**,** 285-295.

TAKASHIMA, Y., GUO, G., LOOS, R., NICHOLS, J., FICZ, G., KRUEGER, F., OXLEY, D., SANTOS, F., CLARKE, J., MANSFIELD, W., REIK, W., BERTONE, P. & SMITH, A. 2014. Resetting Transcription Factor Control Circuitry toward Ground-State Pluripotency in Human. *Cell,* 158**,** 1254-1269.

TAPPONNIER, Y., AFANASSIEFF, M., AKSOY, I., AUBRY, M., MOULIN, A., MEDJANI, L., BOUCHEREAU, W., MAYERE, C., OSTEIL, P., NURSE-FRANCIS, J., OIKONOMAKOS, I., JOLY, T., JOUNEAU, L., ARCHILLA, C., SCHMALTZ-PANNEAU, B., PEYNOT, N., BARASC, H., PINTON, A., LECARDONNEL, J., GOCZA, E., BEAUJEAN, N., DURANTHON, V. & SAVATIER, P. 2017. Reprogramming of rabbit induced pluripotent stem cells toward epiblast and chimeric competency using Kruppel-like factors. *Stem Cell Res,* 24**,** 106-117.

TER HUURNE, M., CHAPPELL, J., DALTON, S. & STUNNENBERG, H. G. 2017. Distinct Cell-Cycle Control in Two Different States of Mouse Pluripotency. *Cell Stem Cell,* 21**,** 449-455 e4.

THEUNISSEN, T. W., FRIEDLI, M., HE, Y., PLANET, E., O'NEIL, R. C., MARKOULAKI, S., PONTIS, J., WANG, H., IOURANOVA, A., IMBEAULT, M., DUC, J., COHEN, M. A., WERT, K. J., CASTANON, R., ZHANG, Z., HUANG, Y., NERY, J. R., DROTAR, J., LUNGJANGWA, T., TRONO, D., ECKER, J. R. & JAENISCH, R. 2016. Molecular Criteria for Defining the Naive Human Pluripotent State. *Cell Stem Cell,* 19**,** 502-515.

THEUNISSEN, T. W., POWELL, B. E., WANG, H., MITALIPOVA, M., FADDAH, D. A., REDDY, J., FAN, Z. P., MAETZEL, D., GANZ, K., SHI, L., LUNGJANGWA, T., IMSOONTHORNRUKSA, S., STELZER, Y., RANGARAJAN, S., D'ALESSIO, A., ZHANG, J., GAO, Q., DAWLATY, M. M., YOUNG, R. A., GRAY, N. S. & JAENISCH, R. 2014. Systematic Identification of Culture Conditions for Induction and Maintenance of Naive Human Pluripotency. *Cell Stem Cell,* 15**,** 471-487.

WADDINGTON, C. H. & WATERMAN, A. J. 1933. The Development in vitro of Young Rabbit Embryos. *J Anat,* 67**,** 355-70.

WANG, S., SHEN, Y., YUAN, X., CHEN, K., GUO, X., CHEN, Y., NIU, Y., LI, J., XU, R. H., YAN, X. & JI, W. 2008. Dissecting signaling pathways that govern self-renewal of rabbit embryonic stem cells. *J Biol Chem,* 19**,** 35929-35940.

WARE, C. B., WANG, L., MECHAM, B. H., SHEN, L., NELSON, A. M., BAR, M., LAMBA, D. A., DAUPHIN, D. S., BUCKINGHAM, B., ASKARI, B., LIM, R., TEWARI, M., GARTLER, S. M., ISSA, J. P., PAVLIDIS, P., DUAN, Z. & BLAU, C. A. 2009. Histone deacetylase inhibition elicits an evolutionarily conserved self-renewal program in embryonic stem cells. *Cell Stem Cell,* 4**,** 359-69.

WIANNY, F., BERNAT, A., MARCY, G., HUISSOUD, C., MARKOSSIAN, S., LEVIEL, V., KENNEDY, H., SAVATIER, P. & DEHAY, C. 2008. Derivation and cloning of a novel Rhesus ES cell line stably expressing tau-GFP. *Stem Cells,* 26**,** 1444-1453.

WU, J., PLATERO-LUENGO, A., SAKURAI, M., SUGAWARA, A., GIL, M. A., YAMAUCHI, T., SUZUKI, K., BOGLIOTTI, Y. S., CUELLO, C., MORALES VALENCIA, M., OKUMURA, D., LUO, J., VILARINO, M., PARRILLA, I., SOTO, D. A., MARTINEZ, C. A., HISHIDA, T., SANCHEZ-BAUTISTA, S., MARTINEZ-MARTINEZ, M. L., WANG, H., NOHALEZ, A., AIZAWA, E., MARTINEZ-REDONDO, P., OCAMPO, A., REDDY, P., ROCA, J., MAGA, E. A., ESTEBAN, C. R., BERGGREN, W. T., NUNEZ DELICADO, E., LAJARA, J., GUILLEN, I., GUILLEN, P., CAMPISTOL, J. M., MARTINEZ, E. A., ROSS, P. J. & IZPISUA BELMONTE, J. C. 2017. Interspecies Chimerism with Mammalian Pluripotent Stem Cells. *Cell,* 168**,** 473-486 e15.

YANG, J., RYAN, D. J., WANG, W., TSANG, J. C., LAN, G., MASAKI, H., GAO, X., ANTUNES, L., YU, Y., ZHU, Z., WANG, J., KOLODZIEJCZYK, A. A., CAMPOS, L. S., WANG, C., YANG, F., ZHONG, Z., FU, B., ECKERSLEY-MASLIN, M. A., WOODS, M., TANAKA, Y., CHEN, X., WILKINSON, A. C., BUSSELL, J., WHITE, J., RAMIREZ-SOLIS, R., REIK, W., GOTTGENS, B., TEICHMANN, S. A., TAM, P. P. L., NAKAUCHI, H., ZOU, X., LU, L. & LIU, P. 2017a. Establishment of mouse expanded potential stem cells. *Nature,* 550**,** 393-397.

YANG, Y., LIU, B., XU, J., WANG, J., WU, J., SHI, C., XU, Y., DONG, J., WANG, C., LAI, W., ZHU, J., XIONG, L., ZHU, D., LI, X., YANG, W., YAMAUCHI, T., SUGAWARA, A., LI, Z., SUN, F., LI, X., LI, C., HE, A., DU, Y., WANG, T., ZHAO, C., LI, H., CHI, X., ZHANG, H., LIU, Y., LI, C., DUO, S., YIN, M., SHEN, H., BELMONTE, J. C. & DENG, H. 2017b. Derivation of Pluripotent Stem Cells with In Vivo Embryonic and Extraembryonic Potency. *Cell,* 169**,** 243-257 e25.

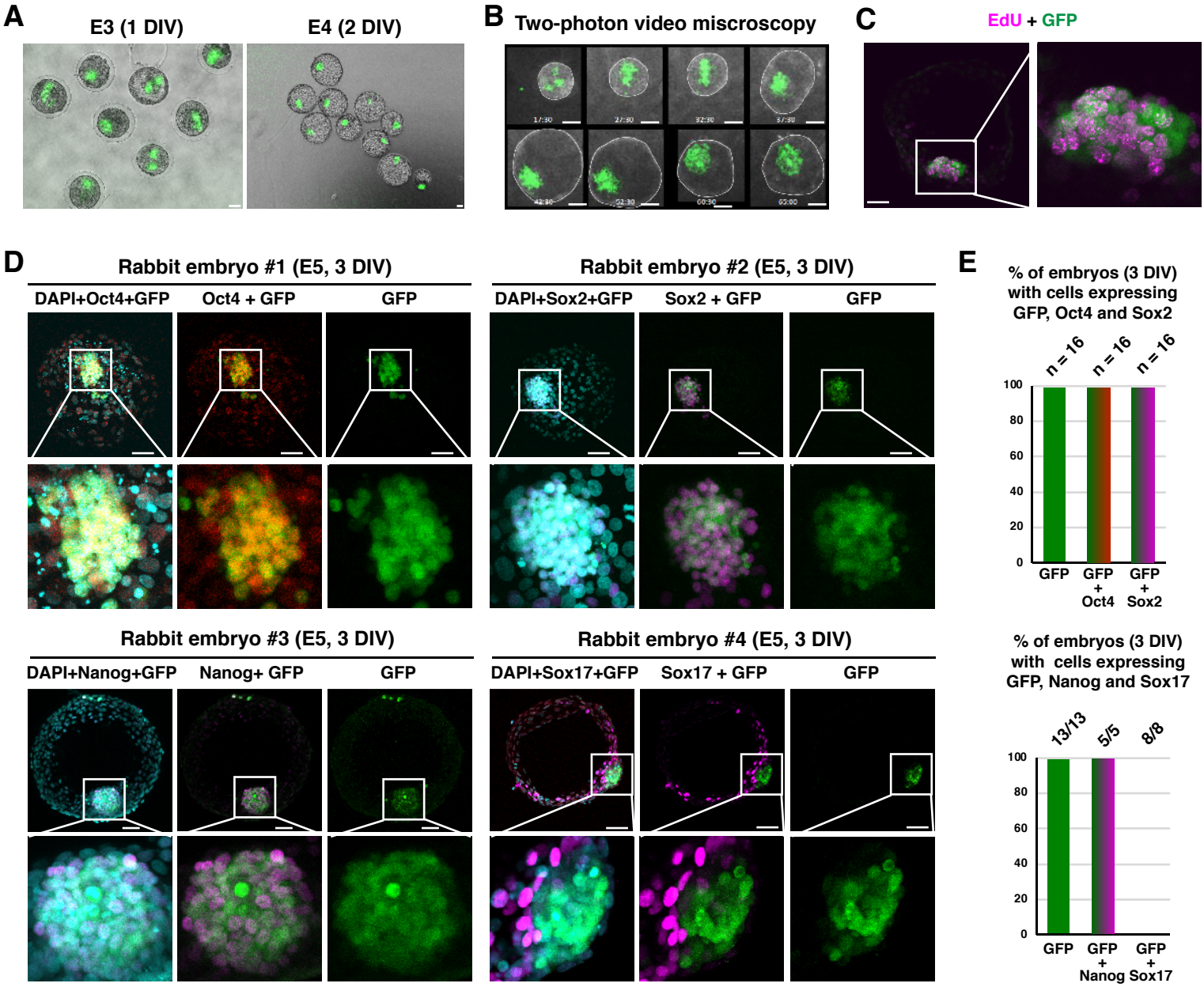
A
E3 (1 DIV)
E4 (2 DIV)
B
Two-photon video miscroscopy
C
EdU + GFP
D
Rabbit embryo #1 (E5, 3 DIV)
DAPI+Oct4+GFP
Oct4 + GFP
GFP
Rabbit embryo #2 (E5, 3 DIV)
DAPI+Sox2+GFP
Sox2 + GFP
GFP
Rabbit embryo #3 (E5, 3 DIV)
DAPI+Nanog+GFP
Nanog+ GFP
GFP
Rabbit embryo #4 (E5, 3 DIV)
DAPI+Sox17+GFP
Sox17 + GFP
GFP
E
% of embryos (3 DIV) with cells expressing GFP, Oct4 and Sox2
n = 16
n = 16
n = 16
100
80
60
40
20
0
GFP
GFP + Oct4
GFP + Sox2
% of embryos (3 DIV) with cells expressing GFP, Nanog and Sox17
13/13
5/5
8/8
100
80
60
40
20
0
GFP
GFP + Nanog
GFP + Sox17
F
Rabbit embryo #6 (E6 in vivo)
GFP
Oct4 + GFP
Sox2 + GFP
Rabbit embryo #7 (E6 in vivo)
Rabbit embryo #8 (E6 in vivo)
Rabbit embryo #9 (E6 in vivo)
Sox17 + GFP
Sox17 + GFP
Sox17 + GFP

Figure 1

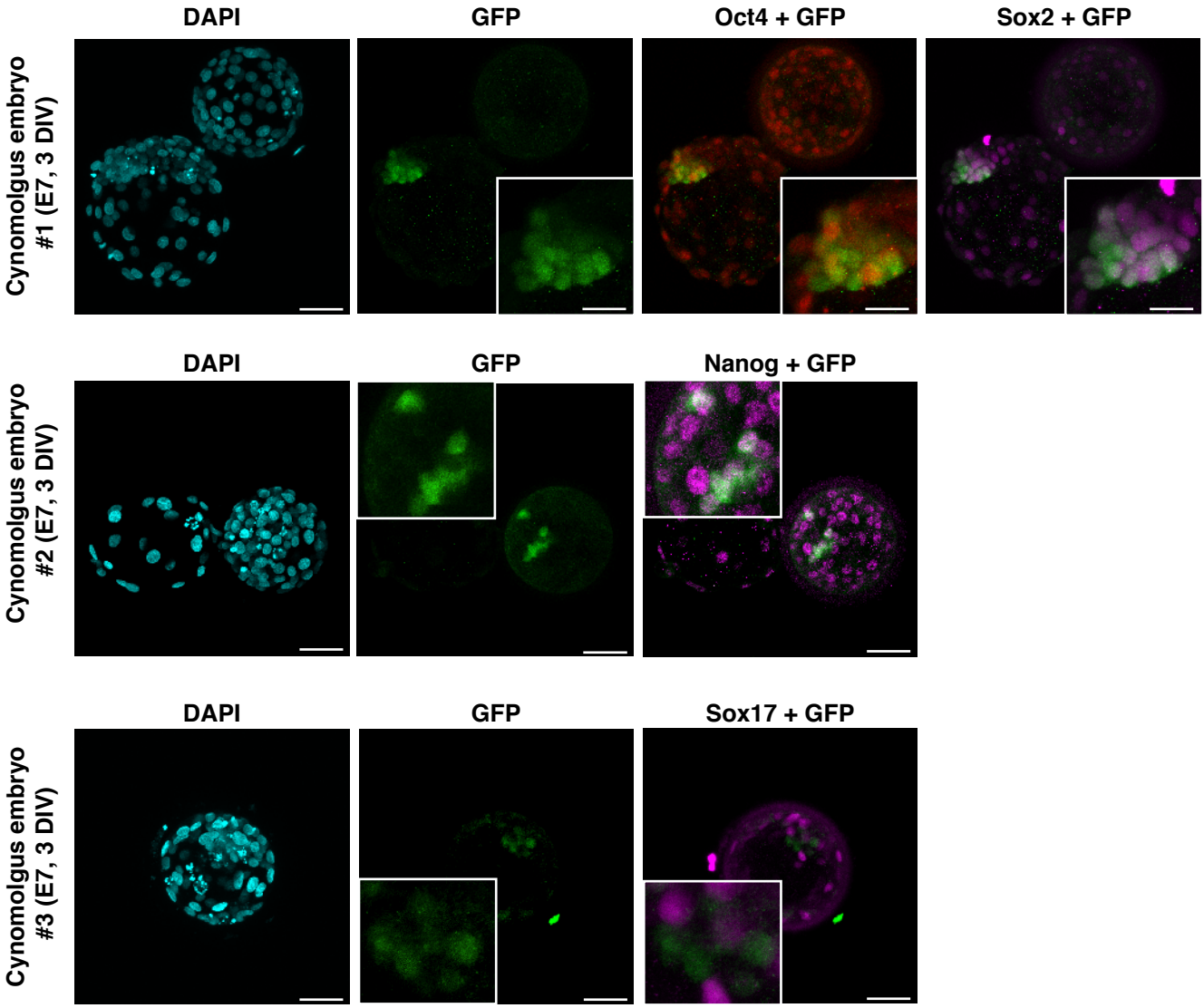
DAPI
GFP
Oct4 + GFP
Sox2 + GFP
Cynomolgus embryo #1 (E7, 3 DIV)
DAPI
GFP
Nanog + GFP
Cynomolgus embryo #2 (E7, 3 DIV)
DAPI
GFP
Sox17 + GFP
Cynomolgus embryo #3 (E7, 3 DIV)

Figure 2

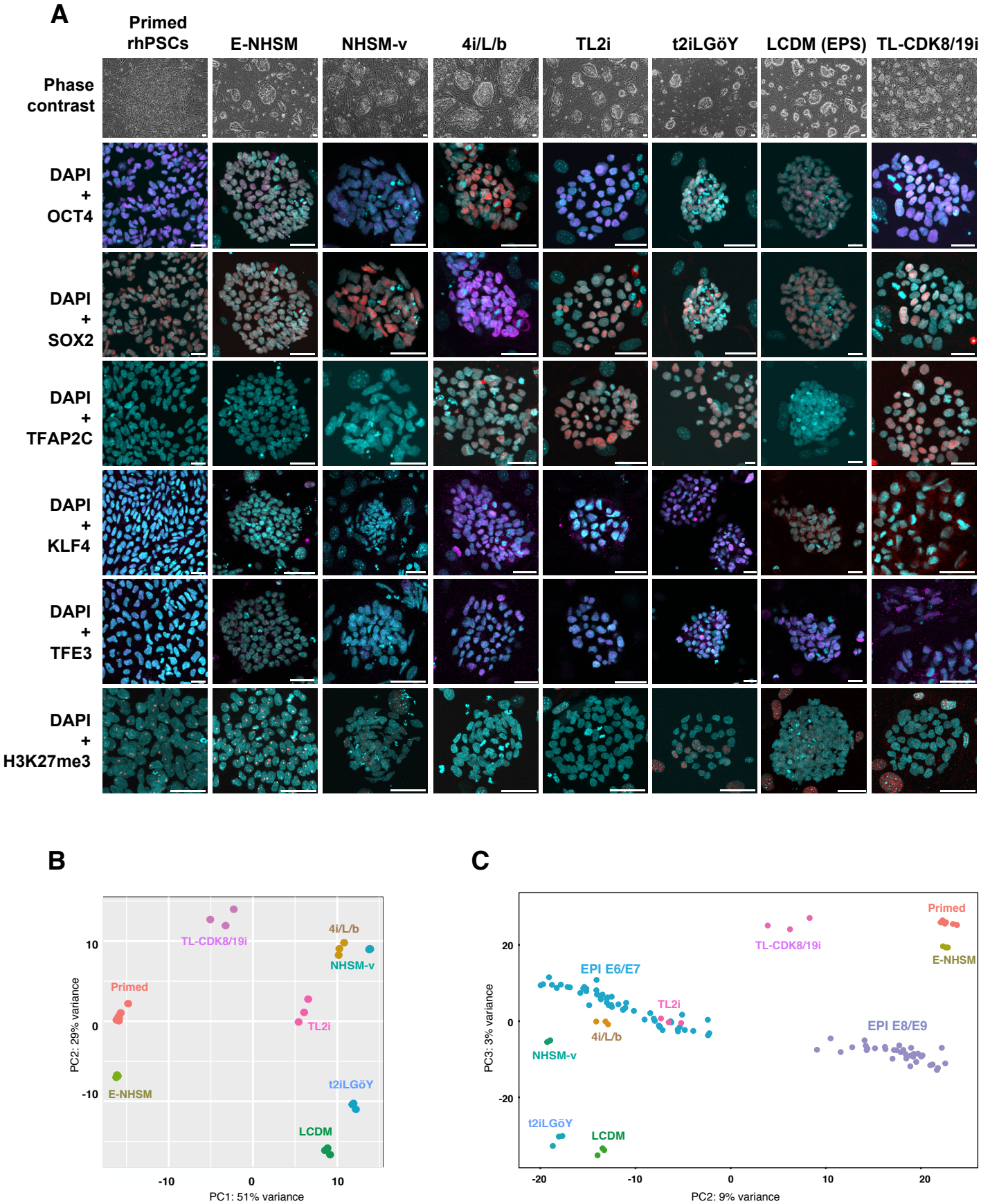
A
Primed rhPSCs
E-NHSM
NHSM-v
4i/L/b
TL2i
t2iLGöY
LCDM (EPS)
TL-CDK8/19i
Phase contrast
DAPI + OCT4
DAPI + SOX2
DAPI + TFAP2C
DAPI + KLF4
DAPI + TFE3
DAPI + H3K27me3
B
TL-CDK8/19i
4i/L/b
NHSM-v
Primed
TL2i
E-NHSM
t2iLGöY
LCDM
PC2: 29% variance
PC1: 51% variance
C
Primed
TL-CDK8/19i
E-NHSM
EPI E6/E7
TL2i
4i/L/b
EPI E8/E9
NHSM-v
t2iLGöY
LCDM
PC3: 3% variance
PC2: 9% variance

Figure 3

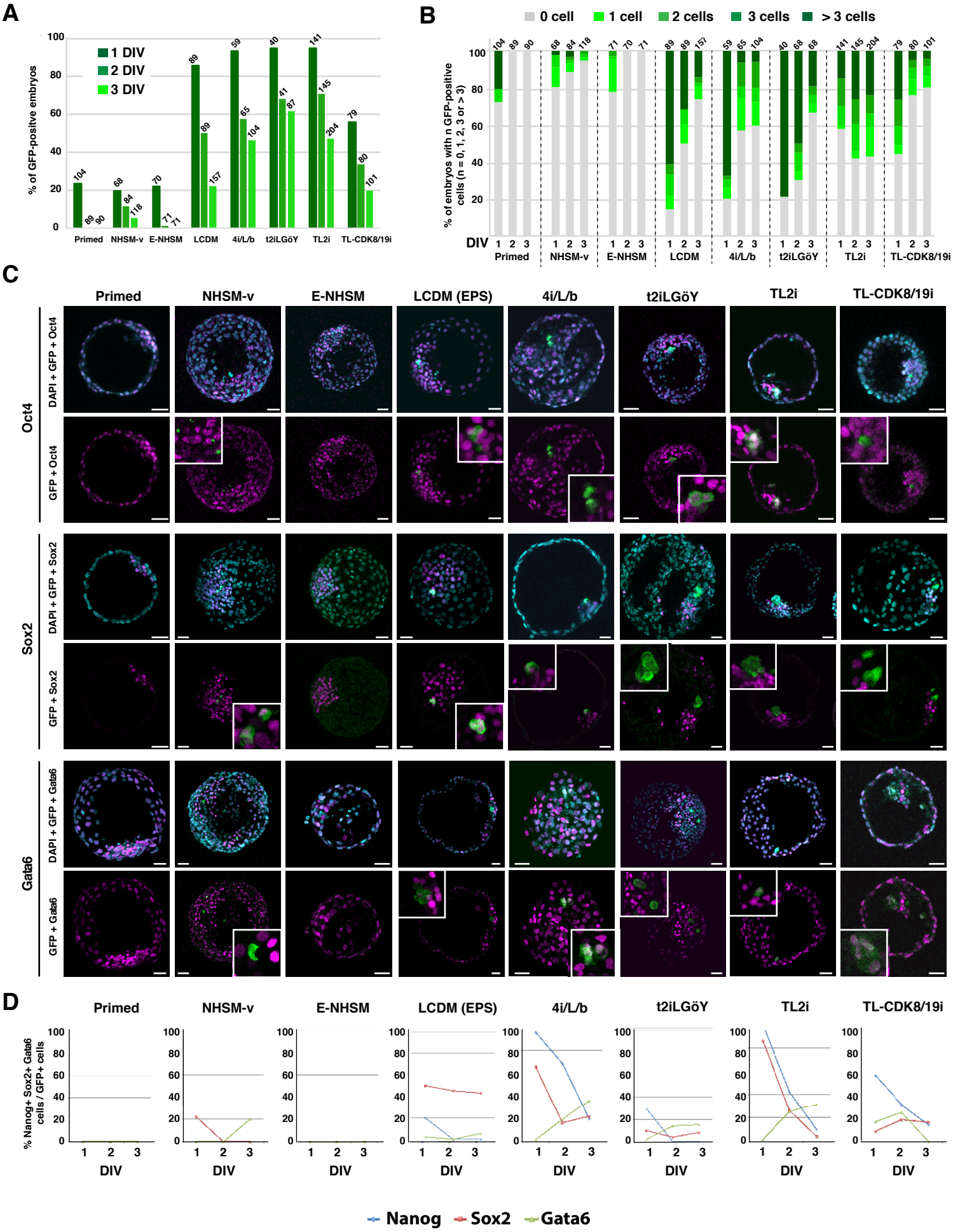
A
% of GFP-positive embryos
1 DIV
2 DIV
3 DIV
Primed
NHSM-v
E-NHSM
LCDM
4i/L/b
t2iLGöY
TL2i
TL-CDK8/19i
B
0 cell
1 cell
2 cells
3 cells
> 3 cells
% of embryos with n GFP-positive cells (n = 0, 1, 2, 3 or > 3)
DIV
C
Primed
NHSM-v
E-NHSM
LCDM (EPS)
4i/L/b
t2iLGöY
TL2i
TL-CDK8/19i
Oct4
DAPI + GFP + Oct4
GFP + Oct4
Sox2
DAPI + GFP + Sox2
GFP + Sox2
Gata6
DAPI + GFP + Gata6
GFP + Gata6
D
% Nanog+ Sox2+ Gata6 cells / GFP+ cells
DIV
Nanog
Sox2
Gata6

Figure 4

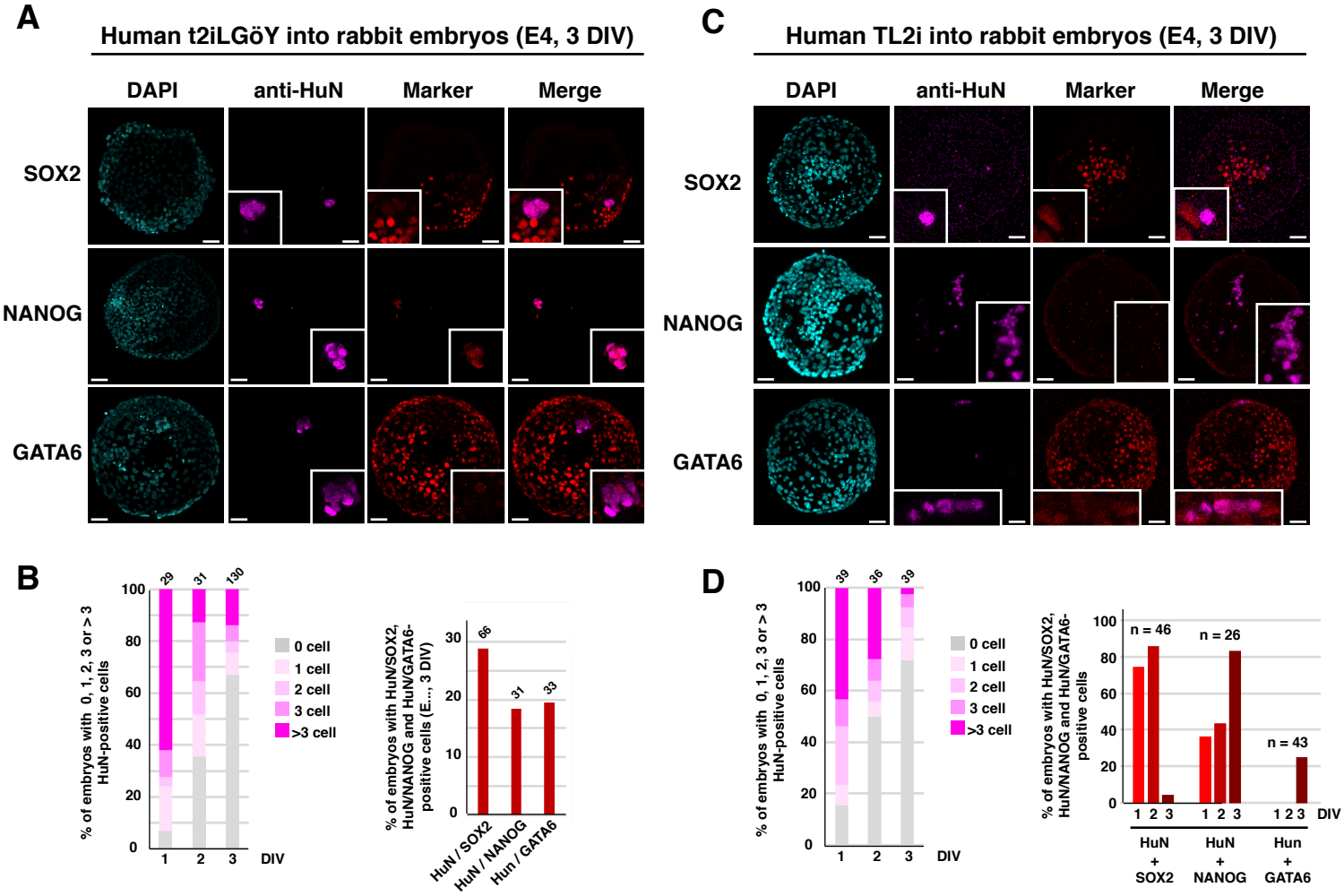
A
Human t2iLGöY into rabbit embryos (E4, 3 DIV)
DAPI
anti-HuN
Marker
Merge
SOX2
NANOG
GATA6
C
Human TL2i into rabbit embryos (E4, 3 DIV)
DAPI
anti-HuN
Marker
Merge
SOX2
NANOG
GATA6
B
% of embryos with 0, 1, 2, 3 or > 3 HuN-positive cells
29
31
130
0 cell
1 cell
2 cell
3 cell
>3 cell
DIV
% of embryos with HuN/SOX2, HuN/NANOG and HuN/GATA6-positive cells (E..., 3 DIV)
86
31
33
HuN / SOX2
HuN / NANOG
Hun / GATA6
D
% of embryos with 0, 1, 2, 3 or > 3 HuN-positive cells
39
36
39
0 cell
1 cell
2 cell
3 cell
>3 cell
DIV
% of embryos with HuN/SOX2, HuN/NANOG and HuN/GATA6-positive cells
n = 46
n = 26
n = 43
DIV
HuN + SOX2
HuN + NANOG
Hun + GATA6

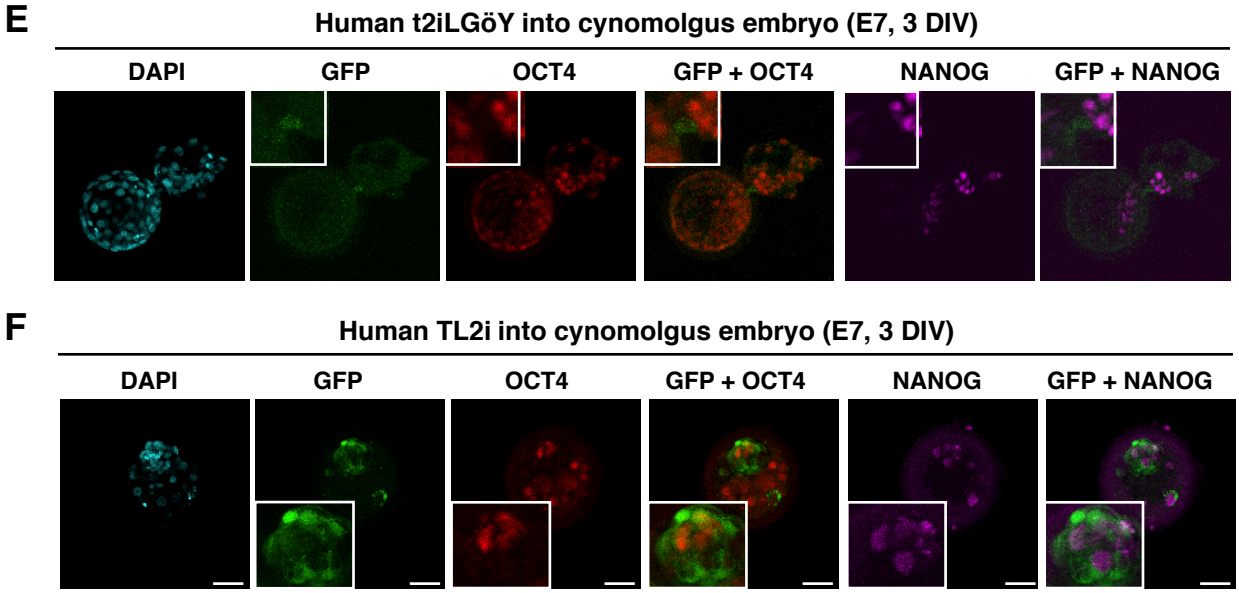
E
Human t2iLGöY into cynomolgus embryo (E7, 3 DIV)
DAPI
GFP
OCT4
GFP + OCT4
NANOG
GFP + NANOG
F
Human TL2i into cynomolgus embryo (E7, 3 DIV)
DAPI
GFP
OCT4
GFP + OCT4
NANOG
GFP + NANOG

Figure 5

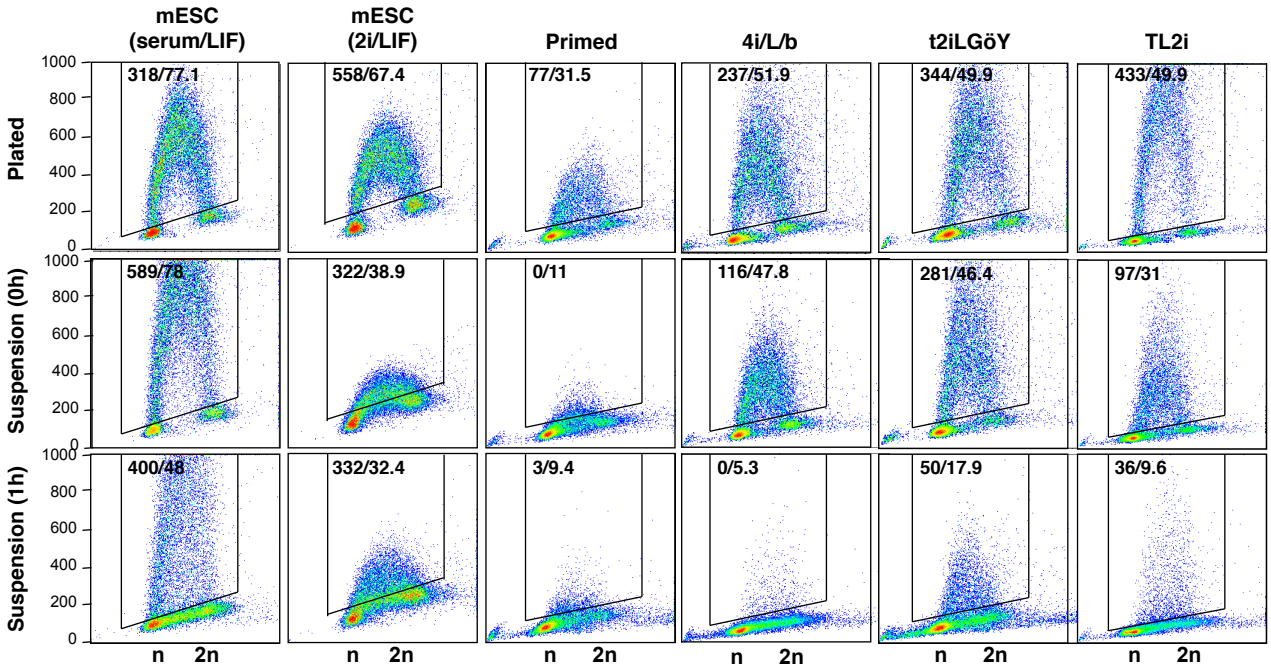
mESC (serum/LIF)
mESC (2i/LIF)
Primed
4i/L/b
t2iLGöY
TL2i
Plated
Suspension (0h)
Suspension (1h)
318/77.1
558/67.4
77/31.5
237/51.9
344/49.9
433/49.9
589/78
322/38.9
0/11
116/47.8
281/46.4
97/31
400/48
332/32.4
3/9.4
0/5.3
50/17.9
36/9.6
1000
800
600
400
200
0
n
2n

Figure 6

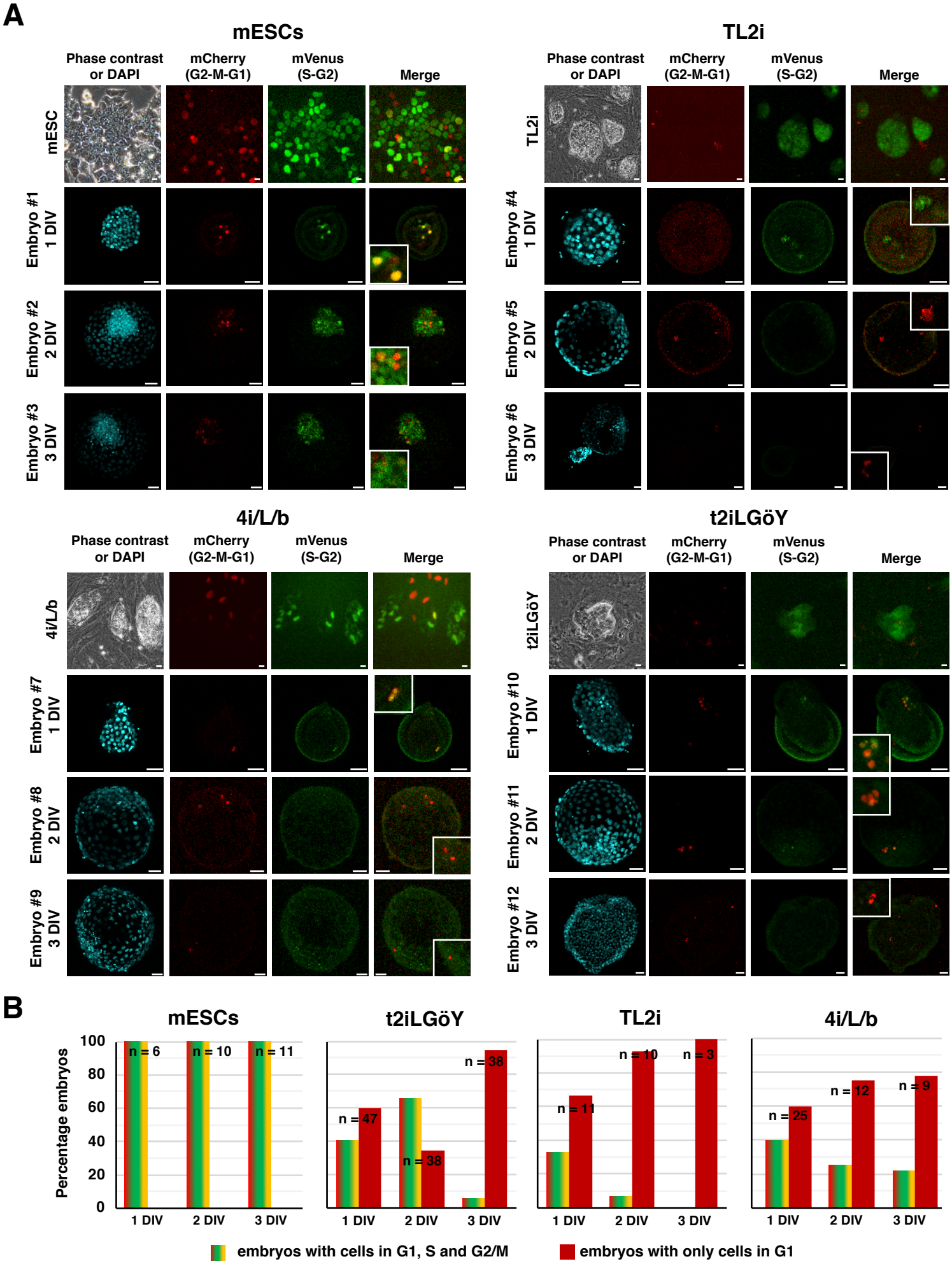
A
mESCs
Phase contrast or DAPI
mCherry (G2-M-G1)
mVenus (S-G2)
Merge
mESC
Embryo #1 1 DIV
Embryo #2 2 DIV
Embryo #3 3 DIV
TL2i
TL2i
Embryo #4 1 DIV
Embryo #5 2 DIV
Embryo #6 3 DIV
4i/L/b
4i/L/b
Embryo #7 1 DIV
Embryo #8 2 DIV
Embryo #9 3 DIV
t2iLGöY
t2iLGöY
Embryo #10 1 DIV
Embryo #11 2 DIV
Embryo #12 3 DIV
B
mESCs
t2iLGöY
TL2i
4i/L/b
Percentage embryos
100
80
60
40
20
0
n = 6
n = 10
n = 11
n = 47
n = 38
n = 38
n = 11
n = 10
n = 3
n = 25
n = 12
n = 9
1 DIV
2 DIV
3 DIV
embryos with cells in G1, S and G2/M
embryos with only cells in G1

Figure 7